

NASA CR-72618

EXPERIMENTAL RESEARCH ON HIGH
FREQUENCY FATIGUE AND DYNAMIC
TENSILE TESTS AT
ELEVATED TEMPERATURES

By

Andrew F. Conn and A. Thiruvengadam

JULY 1969

13495

N70

**CASE FILE
COPY**



HYDRONAUTICS, incorporated
research in hydrodynamics

Research, consulting, and advanced engineering in the fields of NAVAL and INDUSTRIAL HYDRODYNAMICS. Offices and Laboratory in the Washington, D. C. area: Pindell School Road, Howard County, Laurel, Md.

HYDRONAUTICS, Incorporated
TECHNICAL REPORT 829-1

NASA CR-72618

EXPERIMENTAL RESEARCH ON HIGH
FREQUENCY FATIGUE AND DYNAMIC
TENSILE TESTS AT
ELEVATED TEMPERATURES

By

Andrew F. Conn and A. Thiruvengadam

JULY 1969

Prepared for

National Aeronautics and Space Administration
July 1969
Contract NAS3-11168

Technical Management
NASA Lewis Research Center
Cleveland, Ohio
Materials and Structures Division
Gary R. Halford

HYDRONAUTICS, Incorporated
Pindell School Road
Laurel, Maryland

NOTICE

This report was prepared as an account of Government sponsored work. Neither the United States, nor the National Aeronautics and Space Administration (NASA), nor any person acting on behalf of NASA:

- (a) Makes any warranty or representation, expressed or implied, with respect to the accuracy, completeness, or usefulness of the information contained in this report, or that the use of any information, apparatus, method, or process disclosed in this report may not infringe privately owned rights; or
- (b) Assumes any liabilities with respect to the use of, or for damages resulting from the use of any information, apparatus, method or process disclosed in this report.

As used above, "person acting on behalf of NASA" includes any employee or contractor of NASA, or employee of such contractor, to the extent that such employee or contractor of NASA, or employee of such contractor prepares, disseminates, or provides access to, any information pursuant to his employment or contract with NASA, or his employment with such contractor.

Requests for copies of this report
should be referred to:

National Aeronautics and Space Administration
Office of Scientific and Technical Information
P. O. Box 33
College Park, Maryland 20740

HYDRONAUTICS, Incorporated

FOREWORD

The work described herein was performed by HYDRONAUTICS, Incorporated, Laurel, Maryland under NASA Contract NAS3-11168 with the technical management of Dr. Gary R. Halford, NASA Lewis Research Center, Cleveland, Ohio.

TABLE OF CONTENTS

	Page
ABSTRACT.....	iv
SUMMARY.....	1
INTRODUCTION.....	2
HIGH FREQUENCY FATIGUE TESTS.....	5
Fatigue Apparatus.....	5
Experimental Techniques.....	6
DYNAMIC TENSILE TESTS.....	7
Split Hopkinson Pressure Bar Apparatus.....	7
Experimental Techniques.....	7
MATERIALS TESTED.....	10
RESULTS AND ANALYSIS.....	11
High Frequency Fatigue Data.....	11
Dynamic Tensile Properties.....	12
Comparisons of Fatigue Life Prediction Methods.....	13
Four-Point Correlation Method.....	14
Method of Universal Slopes.....	15
CONCLUSIONS AND GENERAL REMARKS.....	17
ACKNOWLEDGMENTS.....	19
APPENDIX A - HIGH FREQUENCY FATIGUE APPARATUS AND TECHNIQUES.....	20
APPENDIX B - COMPONENTS OF SPLIT HOPKINSON PRESSURE BAR APPARATUS.....	27
APPENDIX C - ANALYSIS OF TENSILE IMPACT EXPERIMENTS.....	32
REFERENCES.....	37

LIST OF FIGURES

- Figure 1 - High Frequency Fatigue Apparatus with High Temperature Modification
- Figure 2 - Block Diagram of the Magnetostriction Apparatus Used for High Frequency Fatigue Tests
- Figure 3 - Dumb-Bell Shaped High Frequency Fatigue Specimen
- Figure 4 - Strain Gage Orientation on Fatigue Specimen; BLH Type HT-1212-2A
- Figure 5 - Comparison of Dynamically Measured and Calculated Stresses in 316 Stainless Steel Fatigue Specimens at 1300°F
- Figure 6 - Compressed Gas Gun for Split Hopkinson Bar Apparatus
- Figure 7 - Schematic of Split Hopkinson Pressure Bar Test Facility
- Figure 8 - Principle of Split Hopkinson Pressure Bar Apparatus for Obtaining High Temperature Stress-Strain Data at High Strain Rates
- Figure 9 - High Strain Rate Tensile Specimen
- Figure 10 - High Frequency Fatigue Data for Annealed 316 Stainless Steel at Room Temperature
- Figure 11 - High Frequency Fatigue Data for Annealed 316 Stainless Steel at 1300°F
- Figure 12 - High Frequency Fatigue Data for Titanium 6-2-4-2 Alloy at Room Temperature
- Figure 13 - High Frequency Fatigue Data for Titanium 6-2-4-2 Alloy at 900°F

- Figure 14 - Typical Fractured Tensile Specimens
- Figure 15 - Comparison of High Frequency Fatigue Data with Manson's Fatigue Life Predictions for Annealed 316 Stainless Steel at Room Temperature
- Figure 16 - Comparison of High Frequency Fatigue Data with Manson's Fatigue Life Predictions for Annealed 316 Stainless Steel at 1300°F
- Figure 17 - Comparison of High Frequency Fatigue Data with Manson's Fatigue Life Predictions for Titanium 6-2-4-2 at Room Temperature
- Figure 18 - Comparison of High Frequency Fatigue Data with Manson's Fatigue Life Predictions for Titanium 6-2-4-2 at 900°F
- Figure 19 - Basic Approach for the Design of Dumb-Bell Shaped Fatigue Specimen
- Figure 20 - Compressed Gas Gun Response with Titanium Projectile, Length: 10.5 in., Diameter: 0.752 in., Weight: 0.745 lb.

ABSTRACT

The effects of elevated temperature and high strain rate on fatigue life and tensile properties were measured for annealed 316 stainless steel and titanium alloy 6Al-2Mo-4Zr-2Sn in the solution heat treated and aged condition. A 14 KHz magnetostriction oscillator was used for fatigue testing. A split Hopkinson pressure bar provided dynamic tensile data up to 1300°F. The fatigue data were bracketed by Manson fatigue life predictions, based on static and dynamic tensile properties, although the dynamic prediction curves generally agreed better with data from the highest cycle tests. Creep effects were found to be negligible.

SUMMARY

This technical report summarizes the results of an experimental investigation on the effects of elevated temperature and high strain rates on the fatigue life and tensile properties of two high-temperature materials, and an evaluation of engineering methods for predicting the fatigue behavior of air-breathing engine materials. The two materials studied were annealed 316 stainless steel, and titanium alloy 6Al-2Mo-4Zr-2Sn in the solution heat treated and aged condition.

High frequency fatigue testing was performed on these metals, using a magnetostriction oscillator to produce alternating strains at about 14 KHz in the specimen. This equipment was adapted for operation in excess of 2000°F. A split Hopkinson pressure bar apparatus was designed and constructed for obtaining dynamic tensile properties. Experimental data were obtained at strain rates on the order of 10^3 in./in./sec at temperatures up to 1300°F.

Using the two Manson fatigue life predictions, the four point correlation method and the method of universal slopes, comparisons were made between cyclic lives based on static and dynamic tensile properties. The fatigue data were found to be bracketed by the two calculated curves, although the dynamic prediction curves generally showed better agreement with the data from the highest cycle tests. The role of creep on the high frequency fatigue at elevated temperatures was found to be negligible as predicted by Manson and Halford.

INTRODUCTION

The ever increasing life-time requirements of aerospace engineering systems have called for the accumulation of fatigue life data beyond the practical range of conventional testing equipment. Turbine blades on an air-breathing engine, for instance, rotating at 10,000 rpm for 20,000 hours, would be subjected to 1.2×10^{10} cycles of alternating load. To accumulate this many cycles in a testing machine operating at 10 cycles per second would take about 38 years. Few design engineers could wait that long to settle their material requirements.

With supersonic aircraft being considered for operating lives of 30,000 hours or more, and atomic power-plants which are expected to operate for upwards of 150,000 hours, it becomes clear that new techniques must be developed for quickly evaluating the fatigue properties of various candidate materials (Reference 1). This report summarizes the results of an experimental study of the fatigue behavior of two high temperature alloys. The fatigue lives of these materials were obtained by use of a technique developed at HYDRONAUTICS, Incorporated, which provides high frequency cyclic loading of specimens in various environments and at elevated temperatures, (References 2, 3). With recent modifications, testing is possible at temperatures above 2000^oF. Fatigue data in various hostile and corrosive environments, such as liquid sodium or sea water, and at high pressures have been obtained with this facility. At the frequency of 14 KHz used for these experiments, a billion cycles may be accumulated in only 20 hours, making this technique an extremely useful tool for obtaining practical engineering data.

In addition to obtaining fatigue life data at room temperature and at elevated temperatures, with measured cyclic lives from 10^5 to 10^9 cycles, this study has also examined the influence of high strain rates on fatigue life. Recently engineering methods have been developed for prediction of fatigue lives, based on the tensile properties of materials. Excellent agreements have previously been obtained, for low frequency data up to a million cycles, with two fatigue life prediction methods developed by Manson (References 4,5). These predictions, the four-point correlation method and the method of universal slopes, require calculations which use the ultimate tensile strength, true fracture strength, reduction of area, and elastic modulus. However, application of these methods has been based, until now, on static tensile testing results. In the present research program both static and high strain rate tensile properties were determined and used to calculate fatigue life predictions from the two Manson methods. These predictions were then compared with the high frequency (and therefore high cyclic strain rate) fatigue data.

The dynamic tensile properties were obtained from experiments conducted on a split Hopkinson pressure bar apparatus. The earliest version of this method of studying dynamic events was created by Hopkinson (6). Davies' (7) study of the technique provided a thorough background for the subsequent developments. The first actual split bar experiments were conducted by Kolsky (8). Many recent investigators have refined the analytical and experimental procedures. These include Lindholm (9,10), Hauser, et al. (11), Davies and Hunter (12), and Rand (13).

An interest in determining the effect of superimposing high temperature environments on a high rate of loading has occupied many investigators. Manjoine and Nadai (14,15) pioneered such research, using rather long tensile type specimens which were struck by hammers projecting from a large, spinning flywheel. Stress measurements were made outside the heated area, at a position quite remote from the gage area of the test specimens. Testing of materials at moderate strain rates (less than 100 sec^{-1}) with elevated temperatures has been quite common. Typical is the compression study by Alder and Phillips (16). Moon and Campbell (17) have made a compilation of the tensile, low strain testing literature for metals. High temperature compression tests at impact rates of deformation have been conducted by Bell (18), Chiddister and Malvern (19), Lindholm and Yeakley (20), and recently by Watson and Ripperger (21). In all of the above studies except the last either the stress, the strain, or both were not measured at the elevated temperature.

In the present study, tensile specimens of the type developed by Lindholm and Yeakley (20) were used. To eliminate the approximations necessitated by raising only the test specimen to the elevated temperature, a furnace was made which was large enough to entirely encase both pressure bars. Therefore, no thermal gradients were encountered by the stress waves in these bars, which simplified the interpretation of the data. These results represent the first time correlations have been made between dynamic tensile properties measured at very large strain rates and the high frequency, high cycle fatigue life of elevated temperature alloys. Similar studies have been made (see for instance References 33 and 34) at much lower rates of loading.

HIGH FREQUENCY FATIGUE TESTS

Fatigue Apparatus

Gaines (Reference 22), who introduced the idea of using magnetostriction oscillators for cavitation damage testing, also suggested the use of the same equipment for fatigue testing as well. He, in fact, carried out a few fatigue tests in his apparatus. However, this technique did not gain popularity until Mason (Reference 23), and Neppiras (Reference 24), successfully used exponential and stepped-velocity transformers, thereby making the technique more versatile, because high strains can be produced in any metal with moderate power. A detailed discussion of the various aspects involved in this method is given by Neppiras, (References 24, 25).

In essence the apparatus consists of a magnetostriction transducer, an oscillating signal generator, an amplifier, a power supply, a displacement pick-up coil, an oscilloscope, and a frequency counter. In addition, the facility was modified for operation at elevated temperatures. As shown in Figure 1, a cylindrical electrical coil furnace has been incorporated, with power supply and temperature readout, to provide heating of test specimens in excess of 2000^oF. Special extension rods, with suitable heat-shielding to protect the magnetostriction transducer, were developed for these tests. Details of the experimental components, seen schematically in Figure 2, may be found in References 2 and 3, and in Appendix A of this report.

Experimental Techniques

The basis for this high frequency fatigue technique is the creation of longitudinal oscillations in a fatigue specimen at its resonant frequency producing uniaxial, alternating strains. The maximum alternating strains are produced at the node of the resonant specimen. These strains are further amplified by means of a carefully designed dumbbell shaped configuration at the node. The details of the design of the fatigue specimen are fully described in Appendix A. The dimensions for each of the specimens tested in this program are shown in Figure 3. Note the decrease in length for each of the high temperature versions of these specimens. This decrease is required because of the lowering of elastic modulus with temperature, which in turn decreases the wavelength in the specimen.

Calibration of the output from the displacement measuring coil is provided by direct observations of the maximum amplitudes with a microscope. An additional verification of the strain amplitude calculations was obtained from strain gages mounted on the radius section of high temperature type 316 stainless steel specimens. The orientation of these gages is shown in Figure 4. These strain gages, BLH Type HT-1212-2A, were installed by BLH Electronics, Inc., using their Rokide process, and proved to be very satisfactory at 1300^oF. Static calibrations, using a series of dead loadings, and dynamic calibrations at 14.2 KHz

were obtained over a stress range of from 1600 to 3200 psi. Figure 5. shows a comparison of the dynamically measured and the calculated stresses in these specimens.

DYNAMIC TENSILE TESTS

Split Hopkinson Pressure Bar Apparatus

This apparatus consists of a compressed gas gun which accelerates an impact projectile, two elastic pressure bars to receive and transmit stress waves to and from the test specimen, and electronic equipment for measuring the velocity of the projectile and the stress wave components in the pressure bars. A large furnace, entirely encasing the specimen and both pressure bars, is used to provide elevated temperatures to 1500^oF.

The compressed gas gun is shown in Figure 6. Nitrogen was the gas used to propel the cylindrical projectiles, which were machined for a close sliding fit inside the barrel. A schematic of the complete test facility is given in Figure 7. A photo-electric device is used to measure the projectile velocity. Two high risetime oscilloscopes with Polaroid cameras are used to display and record the output from strain gages on the pressure bars. Detailed descriptions of the components of the split Hopkinson pressure bar apparatus are given in Appendix B.

Experimental Techniques

This technique is based on the measurement of elastic strain waves which are transmitted through a system consisting of two long pressure bars with the test specimens sandwiched between them.

A schematic of this configuration is shown in Figure 8. A projectile impacts the first elastic bar, known as the input bar, creating the incident strain pulse, ϵ_I . Upon reaching the specimen, this incident pulse is partially reflected, as shown by ϵ_R in Figure 8. The second pressure bar, the output bar, receives a transmitted strain pulse, ϵ_T . Each strain wave component is measured by strain gages placed fore and aft of the specimen. From the two strain-time histories recorded by these gages, the strain, stress, and strain rate in the test specimen may be calculated.

Assuming negligible radial inertia forces in the specimen, and with a small coefficient of friction between the faces of the specimen and load bars, it can be shown (see Reference 9, 10 or 11) that the following relationships may be used:

$$\sigma_s = \frac{EA}{2A_s} (\epsilon_I - \epsilon_R + \epsilon_T) \quad [1]$$

$$\epsilon_s = \frac{c}{L_s} \int_0^t (\epsilon_I + \epsilon_R - \epsilon_T) dt \quad [2]$$

$$\dot{\epsilon}_s = \frac{c}{L_s} (\epsilon_I + \epsilon_R - \epsilon_T) \quad [3]$$

where

- σ_s - average stress in specimen
- ϵ_s - average strain in specimen
- $\dot{\epsilon}_s$ - average strain rate in specimen

- L_s - original length of specimen
- A_s - original area of cross section of specimen
- A - area of cross section of pressure bars
- E - elastic modulus of pressure bars
- c - elastic wave velocity in pressure bars, and
- t - time.

In these equations all signs relating to tension, compression, and wave directions have been accounted for, so that absolute values of each strain wave component must be used. The above equations may be suitably modified to account for the use of different materials and different areas of cross section for the two pressure bars. These modifications were required for the high temperature versions of these tests, wherein a larger bending resistance was needed in the input bar. Details of these modifications are given in Appendix C.

The input bar for these tensile tests was actually a hollow, thick-walled tube. The inside diameter was machined to accept the insertion of the tensile impact specimen. This unique specimen, originated by Lindholm (20) is shown in Figure 9, along with the dimensions and tolerances used. The four "legs" of this specimen allow four simultaneous tensile tests to be conducted with each impact. The output bar is a solid cylinder with diameter machined to just fit into the inner diameter of the tensile specimen.

Axial alignment of the projectile and the input bar was made with the projectile partially within the gun barrel. The output bar was then aligned to the input bar, using a removable insert in the input bar. The specimen was then inserted between the two pressure bars. During the impact the pressure bars were free to slide axially along their supports. A "throw bar", identical to the projectile was positioned directly behind the output bar, and captured most of the momentum imparted to the pressure bars. In this manner, motion of the pressure bars was minimized, while the throw bar was caught in a bed of foamed plastic.

The three functions $\epsilon_I(t)$, $\epsilon_R(t)$, and $\epsilon_T(t)$ appearing in Equations [1], [2] and [3] must be determined so that the stress and strain in the specimen may be derived. To determine these functions a digital approach was employed, making use of a computer to reduce the data and plot the results.

MATERIALS TESTED

Two high temperature alloys were tested during this program, under fatigue and tensile impact conditions: annealed 316 stainless steel and titanium alloy 6Al-2Mo-4Zr-2Sn. Both materials were obtained as 3/4-in. diameter bar stock, and all test specimens were machined from the stock "as received", with no further heat treatments.

The 316 stainless steel was supplied by NASA-Lewis. Nominal static mechanical properties for this material, at room temperature and at 1300°F were obtained from Reference 26 and are listed in Table 1.

The Ti-6-2-4-2 alloy was obtained from Titanium Metals Corporation of America, in the solution-treated and aged condition. This condition specifies for the metal to be heated to 1750°F for one hour and air cooled to room temperature, followed by 1100°F for eight hours and air cooled to room temperature. The room temperature and 900°F static mechanical properties were supplied by the manufacturer and are given in Table 2.

The dynamic elastic modulus of both the test materials were experimentally determined at room temperature and at elevated temperature using the fatigue apparatus as explained in Appendix A (see equations A2 and A3). The results are shown in Tables 1 and 2.

RESULTS AND ANALYSIS

High Frequency Fatigue Data

The results of the high frequency, high cycle fatigue tests on 316 stainless steel and Ti-6-2-4-2 alloy are summarized in Table 3 and in Figures 10 through 13. Each experimental point on these figures represents a separate fatigue test. The time to failure for each test specimen was determined when a crack forms in the specimen which is characterized by the increased power level required to maintain a constant displacement amplitude. This amplitude is constantly monitored on an oscilloscope, and for short duration tests the time is measured by stop watch while

the operator visually follows the signal. For longer times an automatic cut-off was used, which turns off the power when the crack has grown large enough so that the power supply can no longer drive the fatigue specimen because of increased damping due to the crack. This also stopped an electric timer. Testing was stopped on specimens which attained 10^9 cycles, and this time is designated as "run out" time.

The number of cycles to failure is computed by multiplying the time to failure and the frequency. This determination differs from the conventional fatigue testing where the specimen breaks into two pieces. In these high frequency fatigue tests the crack has grown to nearly half of the cross section when the increase in power is observed. The test specimens are then easily broken into two pieces by hand if crack observation is desired.

Dynamic Tensile Properties

The results of the tensile impact tests conducted at room temperature, at 1300°F on the 316 stainless steel, and at 900°F with the Ti-6-2-4-2 titanium alloy are summarized in Tables 1 and 2. Note the increases of the ultimate strength, when comparing the dynamic to the static values. In contrast, a decrease of both the dynamic reduction of area and elongation is seen in nearly every case. The sole exception is the dynamic RA for 316 stainless steel, which is 1.19 times larger than the corresponding static value at 1300°F . Another observation made in comparing these static and dynamic properties is the similarity in the ratios of decrease of both RA and elongation, with the exception of the 1300°F values for 316 stainless steel. At room temperature, identical ratios of 0.68 are seen for the stainless steel,

while the titanium alloy ratios for these two properties differ by less than 5 percent at both temperatures. Details of the determinations of reduction of area and elongation are given in Appendix C.

The similarities in the ratios of increase of ultimate stress for the titanium shown in Table 2, at room temperature and at 900°F, as well as the relatively small variation in ratios of decreases of RA and elongation indicate the constancy of rate influence upon this material over the observed temperature range.

The dynamic behavior of 316 stainless steel, however, shows a definite temperature influence. Comparing the ratio columns in Table 1 at room temperature, and at 1300°F, one clearly sees the larger strain rate effect on each property at the elevated temperature. Some typical fractured specimens are shown in Figure 14.

Comparisons of Fatigue Life Prediction Methods

Comparisons of the measured fatigue lives with the two Manson fatigue life predictions are shown in Figures 15, 16, 17 and 18, for annealed 316 stainless steel and Ti-6-2-4-2 alloy. Static and dynamic parameters used to calculate the various prediction curves are listed in Tables 1 and 2. The procedures followed for these predictions by the four-point correlation method and the method of universal slopes are fully described in References 4 and 5. Brief outlines of these prediction methods will be given here.

Four-Point Correlation Method

This method requires the construction of two straight lines, each drawn through two points. These points are plotted in a logarithmic coordinate system with the x-axis as log (number of cycles to failure) and the y-axis as log (total strain range). Letting P_1 and P_2 be the two points required to locate the elastic line, and P_3 and P_4 the points for the plastic straight line, the (abscissa, ordinate) coordinates are as follows

$$\begin{aligned} P_1 & : (1/4, 2.5 \sigma_f) \\ P_2 & : (10^5, 0.9 \sigma_{ult}/E) \\ P_3 & : (10, 1/4 D^{\frac{3}{4}}) \\ P_4 & : \left(10^4, \frac{0.0132 - \epsilon_{el}^*}{1.91} \right) \end{aligned}$$

where σ_u is the measured ultimate stress, E is the elastic modulus; and the true fracture stress, σ_f , and the logarithmic ductility, D , are calculated from

$$\begin{aligned} \sigma_f & = \sigma_u (1 + D) \\ D & = \ln \left(\frac{1}{1 - RA} \right) \end{aligned}$$

The value of ϵ_{el}^* , required to locate point P_4 is obtained from the elastic line. This line must be drawn first, and ϵ_{el}^* then located as the ordinate at the point where the line crosses 10^4 cycles.

Method of Universal Slopes

This prediction method also requires the construction of two lines, an elastic and a plastic line, on the same coordinate system as above, but utilizes a point-slope procedure. The coordinates of the points P_e and P_p , through which the elastic and plastic lines, respectively, are constructed are:

$$P_e : (1, 3.5 \sigma_u/E)$$

$$P_p : (1, D^{0.6}),$$

and the slopes for the elastic and plastic lines are -0.12 and -0.6 respectively.

In each of the figures showing comparisons of the measured data with the static and dynamic versions of one of the prediction methods, the data are seen to be bracketed in general by the static prediction on the low side and the dynamic on the high side. Also, in every case, the data have a slope which is much shallower than the prediction curves. However, the dynamic-based predictions give the best agreement with the highest cycle fatigue tests, in the region of 10^8 - 10^9 cycles.

As predicted by the fatigue life correction formula developed by Manson and Halford (Reference 28) the role of creep was clearly seen to be negligible in these high frequency fatigue experiments. This formula for N_f' , the corrected fatigue life prediction, is

$$N_f' = \frac{N_f}{1 + \frac{k}{AF} (N_f)^{\frac{m+0.12}{m}}} \quad [4]$$

where

- k = effective fraction of each cycle for which the material may be considered to be subjected to the maximum stress,
- F = frequency of stress application, cycles per minute,
- A = coefficient characterising a time intercept of the creep-rupture curve of the material at test temperature. The curve of stress, σ_r , against rupture time, t_r , is linearized on logarithmic coordinates, and represented by the equation $\sigma_r = 1.75\sigma_u (t_r/A)^m$, so that A is the time intercept at an extrapolated value of $\sigma_r = 1.75 \sigma_u$,
- m = slope of creep-rupture line (negative value), and
- N_f = life calculated from either of the two Manson methods discussed above.

The large values of F and N_f in the present experiments made N_f' indistinguishable from N_f .

CONCLUSIONS AND GENERAL REMARKS

As a result of these studies, the following conclusions may be drawn:

1. The split Hopkinson pressure bar technique can be adapted to generate high strain rate tensile data on engineering materials at elevated temperatures.

2. The fatigue data were found to be bracketed in general by the static and dynamic predictions (using both of the Manson fatigue life prediction methods, namely the four point correlation method and the method of universal slopes)(4,5). The dynamic prediction curves generally showed better agreement with the data from the highest cycle tests.

3. The role of creep on the high frequency fatigue at elevated temperatures was found to be negligible as predicted by the Manson-Halford formula (28).

The following general remarks are pertinent to these studies. The high cycle fatigue life curves for both annealed 316 stainless steel and Ti-6-2-4-2 showed small but definable slopes over the range from 10^6 to 10^9 cycles. Such small slopes are to be expected at these life cycle ranges. (See for example Reference 5, page 156, Figure 4.20; Reference 29, page 42, Figure 3.055 and 3.056; References 30 and 31).

The measurement of strain amplitude and the time to failure in the cycle range of less of 10^6 is not very accurate mainly because it takes less than 10 seconds to accumulate 10^5 cycles

and less than 100 seconds to accumulate 10^6 cycles. At such short intervals of time it is very difficult for the experimenter to observe the strain amplitude and the time to failure accurately. It is important to have this limitation in mind when we consider the correlation between the prediction methods and the experimental data. At the high cycle range where this experimental technique is accurate, the correlation is considered to be good. With the exception of the room temperature 316 stainless steel data points, which lie above both prediction curves at the highest life-times, the static and dynamic predictions derived by either method provide lower and upper bounds to the actual high cycle behavior.

The influence on the prediction curves of dynamic effects is clearly seen by comparing fatigue lives calculated from static and from dynamic tensile properties. The bracketing of the data by these curves is seen to be consistent with strain rate effects, when one observes that the static tensile properties are measured at rates less than 10^{-1} in./in./sec.; the dynamic on the order of 10^3 in./in./sec; while the high frequency fatigue measurements on 10^2 in./in./sec. These results emphasize the necessity of understanding the role of rate effects on the fatigue life of materials, particularly at elevated temperatures. The exposure in actual service, such as in turbine or combustion engines, of metals to the combined rigors of high temperatures, high strain rate, and extremely long term cyclical loading present crucial design questions which can only be answered by the establishment of high frequency fatigue testing techniques and prediction methods.

A continued careful development of the techniques applied in the investigation reported here hold promise of providing the required understanding of high cycle, high temperature fatigue behavior, and pave the way for techniques of measurement and prediction which will provide, economically and quickly, practical fatigue life design data up to billions of cycles. The magnetostriction technique permits fatigue testing under any combination of hostile environments, and the superposition of steady or varying loads and thermal fluctuations. The parallel study of dynamic tensile properties is required to complete the understanding of strain rate effects, which is needed to develop high frequency, high cycle fatigue life prediction methods.

ACKNOWLEDGMENTS

The authors wish to express their appreciation to S. Lee Rudy for his work in conducting the high frequency fatigue experiments, and his assistance with the tensile impact testing. The assistance of Robert S. Bowen and Edward W. Russell, Jr., in the experimental work, and Elinor S. Conn in the data reduction is also gratefully acknowledged.

APPENDIX A

HIGH FREQUENCY FATIGUE APPARATUS AND TECHNIQUES

Components

The various components of this apparatus are shown in Figure 2. The high frequency signal from the audio oscillator is amplified and sent to the magnetostriction nickel transducer stack. An exponential velocity transformer is attached to the magnetostriction transducer. The resonant frequency of the system can be changed by varying the length of that portion of the velocity transformer from the nodal support to the free end by means of extension rods. The amplitude is monitored by a suitable voltage pickup coil located approximately midway between the node and the antinode. A permanent magnet is used in the immediate vicinity of the coil to increase the induced voltage. This induced voltage is proportional to the displacement amplitude and the instrument is calibrated by measuring the displacement at the antinode with a filar microscope. The accuracy of these measurements is discussed later.

A detailed study of the transducer system showed that the best quality factor was obtained at 14.2 KHz and hence this frequency was selected for fatigue tests. The quality factor is defined as the ratio of usable energy stored in the system to the total input energy and is given by (32),

$$Q = \frac{\sqrt{3}}{\pi} \frac{f_n}{\Delta f} \quad [A1]$$

where f_n is the resonant frequency and Δf is the width of the resonant curve at half of the maximum amplitude.

Design of Test Specimen

The basic principle of the design of the high frequency fatigue specimens is as follows: When a longitudinal vibration of a half wavelength of a metallic rod is produced by means of an oscillator, the maximum strain is produced at the node while the maximum velocity and displacement are produced at the antinodes at either end of the rod. If a notch is produced at the node, then the strain is further amplified at the node. It is necessary to amplify the strains by means of a notch because of the power limitations of the driving oscillator.

To set up the test, one must attach a half wavelength of rod of specimen material to the free end of the exponential horn and vibrate it at the best frequency selected from considerations of the quality factor. The half wavelength can be experimentally determined by adjusting the rod length to resonate at the best frequency. An accurate determination of this length and frequency will give the value of velocity of sound for each of the metals tested by the relationship

$$c = \lambda f_n \quad [A2]$$

where

- λ is the wavelength,
- f_n is the resonant frequency, and
- c is the velocity of sound.

The modulus of elasticity also can be calculated after determining the density of the metals by the conventional water displacement method, by

$$E = \rho c^2 \quad [A3]$$

where

- E is the modulus of elasticity
- ρ is the density of the metal.

The basic approach for the design of the fatigue specimen is to use the theory developed by Neppiras (24). From this theory one can get the lengths of the fatigue specimen as shown by the example in Figure 19. Assuming an area ratio and l_1/λ , the value of l_2/λ may be determined from Neppiras' theory. In order to avoid the sharp corners, a circular arc fillet of radius R is used. The value of R can be calculated from simple geometrical considerations. This method of designing dumb-bell shaped fatigue specimens gave the dimensions within 10 to 15 percent accuracy. Then the final adjustments are made by tuning experimentally. The dimensions of the properly tuned fatigue specimens are shown in Figure 3.

In all the fatigue studies, theoretical strain, given by the following formula (due to Neppiras 24), was assumed to be the actual value:

$$\epsilon = \frac{G \cdot 2\pi\xi}{\lambda} \quad [A4]$$

where

- ϵ - the strain amplitude at the node,
 - ξ - the displacement amplitude at the antinode,
 - λ - the wavelength in the material, and
 - G - Magnification Factor
- $$= \frac{\text{Strain in stepped specimen}}{\text{Strain in uniform specimen (without step)}}$$

The value of G can be calculated from Neppiras' theory. Generally one would measure the displacement amplitude ξ and the wavelength λ , and calculate the strain using a theoretical value of G . However, we verified these calculations by measuring the actual strains generated at the node. High temperature strain gages (see main text, also Figure 4) were used to measure these strains.

The fatigue specimens were calibrated statically by using deadweights hanging from the specimen. In order to minimize bending, universal joints were provided fore and aft of the fatigue specimens. Assuming that the static calibration holds good for the dynamic measurements also, the dynamic strains were measured at various displacement amplitudes. A comparison between the measured strains and the calculated strains is shown in Figure 5. This effort proved that the theoretical formula is

accurate for our design. The constancy of G is related to the elasticity of the materials being tested. The high temperature calibrations were extended only to about 3 ksi because of the limitations of the strain gages at these temperatures. However it should be noted that the high temperature fatigue tests were conducted at stress amplitudes well below the elastic limit for these metals. Compare the yield stresses of 22.0 ksi for 316 stainless steel at 1300°F, and 81.0 ksi for Ti-6-2-4-2 at 900°F, and the maximum applied fatigue stresses in these experiments, which were only 12.6 ksi and 30.2 ksi respectively. It is clear that these loads were well within the linear elastic portions of the stress-strain curves.

The stress amplitude, σ_a , is given by:

$$\sigma_a = \epsilon \cdot E \quad [A5]$$

and the total strain range, $\Delta\epsilon$ by:

$$\Delta\epsilon = 2\epsilon = \frac{2\sigma_a}{E} \quad [A6]$$

Amplitude Measurement and Determination of Maximum Strains

As pointed out earlier, the maximum amplitude at the anti-node where the fatigue specimen is attached is monitored by means of a calibrated voice coil located as shown in Figure 2. Since the fatigue specimen forms a half wavelength, its addition does not change either the frequency or the calibration. The voltage developed by the coil is dependent upon the metal used

in the transition section of the transducer. At a displacement amplitude of 3×10^{-3} in., 325 mvolts were developed by the coil with the aluminum transition used for the Ti-6-2-4-2 tests, while outputs of over 30 volts were measured from the stainless steel section used in the 316 stainless steel experiments. These coil output voltages could be measured very accurately with an oscilloscope. The actual displacement of the rod end could be measured to an accuracy of $\pm .02 \times 10^{-3}$ inch with a filar microscope. The error in this measurement of the maximum peak-to-peak displacement amplitude was less than one percent. The accuracy of the frequency counter used for frequency measurement was .01 percent and the entire fatigue testing apparatus remained highly stable within 5 cps up to a maximum of 20 hours. The maximum strain was calculated from these measurements using Equations [A3] and [A4]. This method has proven to be very convenient for monitoring and controlling the strains.

Cooling of Specimens

Without outside cooling, the fatigue specimens can become excessively hot near the node due to internal friction. To avoid this unwanted heating in the room temperature tests, a constant temperature was maintained by directing a flow of tap water upon the nodal area of the specimen. Sufficient flow could be attained to keep the specimen surface as cool as the water. By comparing fatigue behavior using distilled water as a coolant, it has been shown that tap water has no influence on the fatigue life of the metals tested.

Although the surface of the specimen was kept at room temperature, it was conceivable that large thermal gradients could provide a much higher temperature at the axis. To check this we timed the heating of a known volume of water, to obtain the rate of heating during the testing of a specimen. This rate was used in a calculation of the thermal gradient, based on heat conduction only in the radial direction. Using room temperature thermal conductivities, gradients of less than 90°F were calculated, and the inclusion of axial heat conduction would considerably reduce this estimate. At elevated temperatures, the increased values of thermal conductivity provide gradients less than 50°F from the radial heat conduction calculation. The actual thermal gradients in these high frequency fatigue tests are therefore seen to be small enough to have very little effect on the material properties.

APPENDIX B

COMPONENTS OF SPLIT HOPKINSON
PRESSURE BAR APPARATUS

Compressed Gas Gun

The gun used to accelerate the impact projectiles is shown in Figure 6. The barrel is 72 inches long and has an 0.755 inch bore diameter. All components of the gun are rated for operation to 3000 psi. The pressure cylinder, made by Walter Kidde Company, Model No. 840534, is 16 inches long, with a 5-1/2 in. diameter, and has a volume of 300 cu in. The large dial gage used to set the pressure in the cylinder is a Helicoid Gage, Model No. 410. This 8-1/2 in. diameter gage registers from 0 to 1000 psi, with minor subdivisions of 10 psi. The valve used to control the gas in the pressure cylinder, and then to provide a sudden release to accelerate the projectile is an Atkomatic Solenoid Valve, Type HP SS, Model 8304R. This valve is activated from a 110 V. AC relay, which is closed with a manually operated, remotely located push button.

Projectiles and Calibration of Gun

Several impact projectiles were used for these dynamic tensile tests. For the tests on Ti-6-2-4-2 the projectiles were circular cylinders of tool steel, 10 inches long by 0.750 in. diameter. Projectiles with 20 in. length having the same diameter were used for the 316 stainless steel tests. Because of the considerably larger elongation of these stainless steel specimens, the longer projectile length was required to provide a stress

pulse of sufficient duration to produce fracture. Each projectile was provided with a slightly rounded impact face. These spherical faces, with radii about 8 inches, minimize undesirable high frequency components ("ringing") in the input stress pulse.

A typical calibration curve for a titanium projectile is shown in Figure 20. Each data point on this figure is the average of at least three shots, and the scatter was less than ± 1.0 ft/sec over the entire range. The calculated curve of velocities shown in Figure 20 was based on an ideal constant pressure calculation:

$$V = \sqrt{\frac{2sP}{\rho L}},$$

where V is the projectile velocity, L is the projectile length, ρ the projectile density and P the gun pressure. The effective acceleration distance, $s = 46.4$ in., was evaluated by averaging the data obtained from 50 to 500 psi. The experimental points are seen to agree quite well with the calculated velocity curve.

Pressure Bars and Strain Gages

The input pressure bars for these split Hopkinson bar tests were 30-inch long hollow tubes. These tubes were machined from 1/2-in. I.D. Schedule 80 seamless pipe, by reaming out the inside diameter to 0.570 in., so as to accommodate the O.D. of the test specimen. The outside diameters of these tubes were 0.840 in. For the room temperature tests 4130 steel was used for the input bars, while Incoloy 825 was the material for the high temperature tests.

The output bars were solid cylindrical bars, also 30 inches long, with 0.488 inch diameters. Ti-6Al-4V alloy was used for the room temperature testing, and Inconel X750 was used for the elevated temperature experiments.

The strain gages used for the room temperature experiments were Micro-Measurements foil-types, WK-05-125BS-120. Their gage resistance is 120 ohms, nominal gage factor: 2, gage length: 0.125 inch and grid width: 0.053 inch. An epoxy adhesive, BR610, supplied by W.T. Bean, Inc., was used to mount these gages. Two gages were placed at each measuring station on the pressure bars, located 14 inches from the ends of the bars which are in contact with the test specimen. The gage pairs were located on opposite sides of the bars, and operated in series to cancel any strain reading associated with flexure of the load bars. Microdot weldable type strain gages were used for the elevated temperature tensile impact tests. Type MG 120 gages were used, having a flange length of 0.38 inch and width of 0.10 inch. These gages were mounted to the pressure bars by many tiny spot welds applied by a capacitive-discharge welder.

Strain and Velocity Measuring Equipment

Two Tektronix type 561A oscilloscopes were used to display the strain gage output signals. The vertical amplification was provided by type 3A8 and type 2A63 plug-in units. The test traces were photographed by type K-5 Oscilloscope cameras with Polaroid film pack backs. The oscilloscopes were operated in the single sweep mode, and were triggered externally when the projectile struck the input bar.

The strain gages were connected into a potentiometer type of dynamic circuit. Calibration was provided by selection of a precision calibration resistor, which was alternated in parallel with the gages by means of an electronic chopper. The calibration signals were superimposed on the same print which was to contain the dynamic strain signal, to minimize any photographic errors in the data reduction.

The system used to measure the projectile velocity included a small light source, a miniature photo transistor, an electronic counter, and a lock-out circuit to prevent restart of the counter in case the projectile rebounded back into the light field. During passage of the projectile past the light, the darkened photo transistor allowed the counter to register the time of passage. Thus, dividing the projectile length by the time of passage, an average velocity is derived. By repeating this measurement at various venting holes in the barrel, and beyond the muzzle, a region of constant velocity can be determined and the impact can be arranged within this region. The photo transistor was a Motorola type MRD 300, and the counter a Systron-Donner Model 114EEX.

Furnace

The high temperature environment for these impact tests was provided by a furnace which was specially fabricated for this study by Electro-Applications, Inc. The heating elements were

wire-coil type, arranged around a circular cavity 2-3/8 inches in diameter and 61 inches long, which completely contained both pressure bars. Temperature control was provided by a Fenwal Series 524 controller. This furnace is rated for operation to 1500°F. The top is hinged to open in two sections.

APPENDIX C

ANALYSIS OF TENSILE IMPACT EXPERIMENTS

Dynamic Property Calculations Using Unequal Pressure Bars

The equations which are used to calculate the average stress, strain, and strain rate in the test specimen, when the two pressure bars are made of the same material and have equal areas, are given as Equations [1], [2] and [3] in the main text. If there are differences in material and cross sectional area for these two bars, this must be accounted for in the derivation of the equations for stress, strain and strain rate. In the derivation to follow the notation will be the same as that given after Equation [3], with the following additional symbols:

- u_1 - displacement of face of input bar adjacent to specimen,
- u_2 - displacement of face of output bar adjacent to specimen,
- A_1, A_2 - area of cross section of input, output bar,
- E_1, E_2 - elastic modulus of input, output bar, and
- c_1, c_2 - elastic bar velocity in input, output bar.

It may be shown from a one-dimensional analysis of elastic wave propagation that the displacement and strain are related by:

$$u = c \int_0^t \epsilon dt' \quad [C1]$$

The displacement u_1 is caused by ϵ_I and by ϵ_R traveling in the opposite direction (see Figure 8). (Absolute values should be used for strain components when applying these equations).

$$u_1 = c_1 \int_0^t (\epsilon_I + \epsilon_R) dt' \quad [C2]$$

while the displacement on the output face is

$$u_2 = c_2 \int_0^t \epsilon_T dt' \quad [C3]$$

Combining [C2] and [C3] the average strain in the specimen is therefore:

$$\epsilon_s = \frac{u_1 - u_2}{L_s} = \frac{c_1}{L_s} \int_0^t (\epsilon_I + \epsilon_R) dt' - \frac{c_2}{L_s} \int_0^t \epsilon_T dt' \quad [C4]$$

Differentiation of [C4] provides the equation for the average strain rate in the specimen

$$\dot{\epsilon}_s = \frac{c_1(\dot{\epsilon}_I + \dot{\epsilon}_R)}{L_s} - \frac{c_2 \dot{\epsilon}_T}{L_s} \quad [C5]$$

The forces F_1 and F_2 on the input and output faces of the specimen are

$$F_1 = E_1 A_1 (\epsilon_I - \epsilon_R) \quad , \quad F_2 = E_2 A_2 \epsilon_T \quad .$$

Therefore, the average stress in the specimen is:

$$\sigma_s = \frac{F_1 + F_2}{2A_s} = \frac{E_1 A_1}{2A_s} (\epsilon_I - \epsilon_R) + \frac{E_2 A_2}{2A_s} \epsilon_T \quad [C6]$$

If the stress is constant through the thickness of the specimen, reduced forms of Equations [C4], [C5] and [C6] may be used which require measurement only of ϵ_R and ϵ_T

$$\epsilon_s = \frac{2c_1}{L_s} \int_0^t \epsilon_R dt' + \left(\frac{c_1 E_2 A_2}{L_s E_1 A_1} - \frac{c_2}{L_s} \right) \int_0^t \epsilon_T dt' \quad [C7]$$

$$\dot{\epsilon}_s = \frac{2c_1}{L_s} \dot{\epsilon}_R + \left(\frac{c_1 E_2 A_2}{L_s E_1 A_1} - \frac{c_2}{L_s} \right) \dot{\epsilon}_T \quad [C8]$$

$$\sigma_s = \frac{E_2 A_2}{A_s} \epsilon_T \quad [C9]$$

The last three equations were used in the computer program which was created to calculate the dynamic properties of the materials.

Determination of Reduction of Area and Elongation

The complex geometry of the tensile impact specimens required careful measurement of each specimen before and after its test to determine the area and lengths so that reduction of area and elongation could be derived. Diameter measurements were made before testing with micrometers. Slot widths and lengths (see Figure 9) were measured with vernier calipers. With these measurements, the area before testing was calculated using:

$$A_s = \frac{\pi}{4} (D_o^2 - D_i^2) - D_o^2 \left[K_o \sqrt{1-K_o^2} + \tan^{-1} \left(\frac{K_o}{\sqrt{1-K_o^2}} \right) \right] \\ + D_i^2 \left[K_i \sqrt{1-K_i^2} + \tan^{-1} \left(\frac{K_i}{\sqrt{1-K_i^2}} \right) \right] \quad [C10]$$

where

D_o - outside diameter of specimen, nominally 0.55 in.

D_i - inside diameter of specimen, nominally 0.49 in.

$$K_o = \frac{W}{D_o} \quad , \quad K_i = \frac{W}{D_i}$$

W = slot width, nominally 3/16 in.

To determine the area after fracture, each leg was measured, using a microscope which was fitted with a micrometer translating stage. It was found that by measuring the thickness, T , of each leg, and the outer chord length, B , the new outside and inside diameters, D_o' and D_i' , and the new slot width W' could be calculated

-36-

$$D_o' = \frac{1}{2} (D_o + D_i) + T \quad [C11]$$

$$D_i' = \frac{1}{2} (D_o + D_i) - T \quad [C12]$$

$$W' = \left(\frac{D_o'^2 - B^2}{2} \right)^{\frac{1}{2}} - B\sqrt{2} \quad [C13]$$

where it has been found that, to within readable tolerances, the mean diameter does not change, the edges of each leg are still perpendicular, and the thickness of each leg is essentially constant. The results of [C11], [C12] and [C13] may then be used in an equation analogous to [C10] except each individual leg area is calculated. Summing the four areas, a final area A_s' is found, and the reduction of area is given by

$$RA = \frac{A_s - A_s'}{A_s} \times 100 \quad [C14]$$

The elongation was obtained by measuring the specimen leg lengths, L_s , before and L_s' , after the fracture. The L_s' measurement required two people, one refitting the two fractured parts back together and holding them, while the second person measured the length. Using these measurements

$$\text{Elongation} = \frac{L_s' - L_s}{L_s} \times 100 \quad [C15]$$

REFERENCES

1. Manson, S. S., "Design Considerations for Long Life at Elevated Temperatures," James Clayton Lecture NASA Lewis TP. I-63, Presented at the Joint International Conference on Creep Sponsored by Institute of Mechanical Engineers, ASTM and ASME, London, England, 1963.
2. Thiruvengadam, A., "High Frequency Fatigue of Metals and their Cavitation Damage Resistance," HYDRONAUTICS, Incorporated Technical Report 233-6, December 1964. (See also Trans. ASME, Journal of Engineering for Industry, August 1966).
3. Thiruvengadam, A., and Preiser, H. S., "Cavitation Damage in Liquid Metals," HYDRONAUTICS, Incorporated Technical Report 467-Final, NASA CR-72035, November 1965.
4. Manson, S. S., "Fatigue - A Complex Subject - Some Simple Approximations," The William M. Murray Lecture, Experimental Mechanics, Vol. 5, pp. 193-226, 1965.
5. Manson, S. S., Thermal Stress and Low-Cycle Fatigue, McGraw-Hill, New York, 1966.
6. Hopkinson, B., "A Method of Measuring the Pressure Produced in the Detonation of High Explosives or by the Impact of Bullets," Phil. Trans. Roy. Soc. London, Ser. A., Vol. 213, pp. 437-456, 1914.
7. Davies, R. M., "A Critical Study of the Hopkinson Pressure Bar," Phil. Trans. Roy. Soc. London, Ser. A. Vol. 240, pp. 375-457, 1948.
8. Kolsky, H., "An Investigation of the Mechanical Properties of Materials at Very High Rates of Loading," Proc. Phys. Soc. London, Sect. B., Vol. 62, pp. 676-700, 1949.
9. Lindholm, U. S., "An Experimental Determination of the Stress-Strain Rate Relations of Several Metals," Ph.D. Thesis, Michigan State University, 1960.

10. Lindholm, U. S., "Some Experiments with the Split Hopkinson Pressure Bar," J. Mech. Phys. Solids, Vol. 12, pp. 317-335, 1964.
11. Hauser, F. E., Simmons, J. A., and Dorn, J. E., "Strain Rate Effects in Plastic Wave Propagation," Response of Metals to High Velocity Deformation, Proc. Metallurgical Soc. Conf., Vol. 9, Interscience, N. Y., pp. 93-114, 1961.
12. Davies, E.D.H., and Hunter, S. C., "The Dynamic Compression Testing of Solids by the Method of the Split Hopkinson Pressure Bar," J. Mech. Phys. Solids, Vol. 11, pp. 155-179, 1963.
13. Rand, J. L., "An Analysis of the Split Hopkinson Pressure Bar," NOLTR 67-156, U. S. Naval Ordnance Laboratory, White Oak, Maryland, October 1967.
14. Manjoine, M. J., and Nadai, A., "High-Speed Tension Tests at Elevated Temperatures," Proc. ASTM, Vol. 40, pp. 822-839, 1940; Parts II and III: J. Appl. Mech., Vol. 8, Trans. ASME, Vol. 63, pg. A-77, 1941.
15. Manjoine, M. J. "Influence of Rate of Strain and Temperature on Yield Stresses in Mild Steel," J. Appl. Mech., Vol. 11, Trans. ASME, Vol. 66, pg. 211, 1944.
16. Alder, J. F., and Phillips, V. A., "The Effect of Strain Rate and Temperature on the Resistance of Aluminum, Copper and Steel to Compression," J. Inst. Metals, Vol. 83, pp. 80-86, 1954.
17. Moon, D. P., and Campbell, J. E., "Effects of Moderately High Strain Rates on the Tensile Properties of Metals," DMIC Memo 142, Defense Metals Info. Center, Battelle Memorial Inst., Columbus, Ohio, December 1961 (AD-270-167, ASTIA).
18. Bell, J. F., "Experimental Study of Dynamic Plasticity at Elevated Temperatures," Experimental Mechanics, Vol. 1, pp. 181-186, 1962.

19. Chiddister, J. L., and Malvern, L. E., "Compression-Impact Testing of Aluminum at Elevated Temperatures," Experimental Mechanics, Vol. 3, pp. 81-90, 1963.
20. Lindholm, U. S., and Yeakley, L. M., "High Strain-Rate Testing: Tension and Compression," Experimental Mechanics, Vol. 8, pp. 1-9, 1968.
21. Watson, H., Jr., and Ripperger, E. A., "Dynamic Stress-Strain Characteristics of Metals at Elevated Temperatures," Experimental Mechanics, Vol. 9, pp. 289-295, 1969.
22. Gaines, N., "A Magnetostriction Oscillator Producing Intense Audible Sound and Some Effects Obtained," Physics, Vol. 3, pp. 209-229, 1932.
23. Mason, W. P., "Internal Friction and Fatigue in Metals at Large Strain Amplitudes," J. Acous. Soc. America, Vol. 28, pp. 1207-1218, 1956.
24. Neppiras, E. A., "Techniques and Equipment for Fatigue Testing at Very High Frequencies," Proc. ASTM, Vol. 59, pp. 691-709, 1959.
25. Neppiras, E. A., "Metal Fatigue at High Frequency," Proc. Phys. Soc., London, Ser. B., Vol. 70, p. 393, 1957.
26. Sachs, G., editor, "Air Weapons Materials Application, Metals and Alloys," ARDC TR 59-66, Syracuse University, Syracuse, New York, December 1959.
27. Hodge, A. W., and Muykith, D. J., "Properties of New High-Temperature Titanium Alloys," DMIC Memo 230, Defense Metals Info. Center, Battelle Memorial Inst., Columbus, Ohio, February 1968.
28. Manson, S. S., and Halford, G., "A Method of Estimating High-Temperature Low Cycle Fatigue Behavior of Materials," Thermal and High-Strain Fatigue, The Metals and Metallurgy Trust, London, pp. 154-170, 1967. (Also, NASA TM-X-52270, 1967).

29. Aerospace Structural Metals Handbook, Vol. II, Nonferrous Alloys, Belfour Stulen Co., Inc., Trevor City, Michigan, 1968, pg. 42 (original report: D. N. Torell, "Data on Ti-679 and Ti-6Al-2Sn-4Zr-2Mo Titanium Alloys," Pratt and Whitney Aircraft, West Palm Beach, Florida, 12 August 1966).
30. Valluri, S. R., "A Unified Engineering Theory of High Stress Level Fatigue," Aerospace Engineering, Vol. 20, No. 10, pg. 18, October 1961.
31. Harris, W. J., Metallic Fatigue, Pergamon Press Ltd., Oxford, England, 1961.
32. Jensen, J. W., "Damping Capacity -- Its Measurement and Significance," Report of Investigations, Bureau of Mines, U. S. Dept. of Interior, 1959.
33. Coffin, L. F., Jr., "Cyclic Strain and Fatigue Study of a 0.1 pct C - 2.0 pct Mo Steel at Elevated Temperatures," Trans. Met. Soc. AIME, Vol. 230, pp. 1690-1699, 1964.
34. Forrest, P. G., and Armstrong, K. B., "Investigation of the Thermal-Fatigue Behavior of Nickel--Chromium-Base Alloys by Strain-Cycling Tests," J. Inst. Metals, Vol. 94, pp. 204-213, 1966.

TABLE 1
 Static and Dynamic Tensile Properties of Annealed 316 Stainless Steel

Property	Room Temperature			1300°F		
	Static ^a	Dynamic [*]	Ratio ^d	Static ^a	Dynamic [*]	Ratio ^d
Ultimate Tensile Strength σ_u , ksi	81.2	138 ^b	1.63	46.0	109.2 ^b	2.37
Reduction of Area, RA, %	76.9	52.3 ^b	0.68	50.0	59.3 ^b	1.19
Elongation %	55.0	37.3 ^b	0.68	35.0	31.8 ^b	0.91
Logarithmic Ductility ^e , D	1.4653	0.7391	0.50	0.6932	0.8989	1.30
True Fracture Strength _f , σ_f , ksi	200.2	240.0	1.20	76.3	207.4	2.72
Elastic Modulus, E, 10 ⁶ psi	28.4	28.8 ^c	1.01	20.5	19.8 ^c	0.97

a. Values from Reference 26
 b. Split Hopkinson pressure bar experiments
 c. High frequency fatigue experiments
 d. Ratio of dynamic to static value
 e. $D = \ln \left(\frac{1}{1 - RA} \right)$, Refs. 4 and 5
 f. $\sigma_f = \sigma_u (1+D)$, Refs. 4 and 5
 * Strain rate $\approx 10^3$ in./in./sec

TABLE 2
Static and Dynamic Tensile Properties of Titanium Alloy Ti-6-2-4-2

Property	Room Temperature			900°F		
	Static ^a	Dynamic [*]	Ratio ^e	Static ^a	Dynamic [*]	Ratio ^e
Ultimate Tensile Strength σ_u , ksi	152.0	229.5 ^c	1.51	106.0	166.8 ^c	1.57
Reduction of Area, RA, %	44.0	40.3 ^c	0.92	60.3	57.2 ^c	0.95
Elongation, %	17.0	15.1 ^c	0.89	21.0	20.7 ^c	0.99
Logarithmic Ductility, D	0.5805	0.5158	0.89	0.9239	0.8484	0.92
True Fracture Strength ^g , σ_f , ksi	240.2	347.4	1.45	203.9	308.3	1.51
Elastic Modulus, E, 10^6 psi	16.0	16.7 ^d	1.04	11.6 ^b	12.0 ^d	1.03

a. Test value from manufacturer

Titanium Metals Corp. of America

b. Value from Reference 27

c. Split Hopkinson pressure bar experiments

d. High frequency fatigue experiments

e. Ratio of dynamic to static value

f. $D = \ln \left(\frac{1}{1 - RA} \right)$, References 4 and 5

g. $\sigma_f = \sigma_u (1+D)$, References 4 and 5

* Strain Rate $\approx 10^3$ in./in./sec

TABLE 3a
 High Frequency Fatigue Data for Annealed 316 Stainless
 Steel at Room Temperature

Specimen Number	Time to Failure			Cycles to Failure N	Stress ksi	Total Strain Range $\Delta\epsilon \times 10^{-3}$	Freq. KHz
	Hours	Min	Sec				
9			20	2.80×10^5	39.3	2.73	14.0
10			21	2.95×10^5	39.3	2.73	14.0
11		2	34	2.1×10^6	33.8	2.35	14.0
12		1	40	1.4×10^6	33.8	2.35	14.0
1		1	30	1.26×10^6	33.4	2.32	14.0
3		1	40	1.4×10^6	33.4	2.32	14.0
5		1	30	1.26×10^6	33.4	2.32	14.1
6			40	5.6×10^5	33.4	2.32	14.0
4		6	25	5.4×10^6	32.3	2.24	14.0
7		8	25	7.15×10^6	32.3	2.24	14.0
8		2		1.68×10^6	32.3	2.24	14.1
2		13		1.09×10^7	31.2	2.17	14.0
13		6	30	5.5×10^6	31.2	2.17	14.1
15		35	4	2.95×10^7	31.2	2.17	14.1
17	21	47		$1.08 \times 10^{9*}$	29.1	2.02	14.0
20		20	54	1.76×10^7	29.1	2.02	14.0
22	11	21		5.81×10^8	29.1	2.02	14.1
16	27	48		$1.42 \times 10^{9*}$	28.1	1.95	14.2

* Stopped test, specimen did not fail.

TABLE 3b

High Frequency Fatigue Data for Annealed 316 Stainless at 1300°F

Specimen Number	Time to Failure			Cycles to Failure N	Stress, ksi	Total Strain Range $\Delta\epsilon$ $\times 10^{-3}$	Freq. KHz
	Hours	Min	Sec				
Chk			15	2.2×10^5	12.4	1.23	14.1
1			14	2.0×10^5	12.4	1.23	14.1
2			30	4.24×10^5	12.4	1.23	14.1
5	5	7		2.54×10^8	11.9	1.20	14.1
6			22	3.10×10^5	11.9	1.20	14.1
7			33	4.66×10^5	11.9	1.20	14.1
8			43	6.06×10^5	11.6	1.17	14.1
3	8	35		4.36×10^8	11.5	1.16	14.1
4	21			$1.07 \times 10^{9*}$	11.5	1.16	14.1
18		14	56	1.26×10^7	11.5	1.16	14.1
11		9	42	8.21×10^6	11.3	1.14	14.1
15		22	56	1.94×10^7	11.3	1.14	14.1
21	1	3		5.34×10^7	11.3	1.14	14.1
12	2	19		1.2×10^8	11.0	1.11	14.1
13	2	12		1.12×10^8	11.0	1.11	14.1
14	1	25		7.19×10^7	11.0	1.11	14.1
16	1	57		9.91×10^7	10.7	1.08	14.1
17	2			1.02×10^8	10.7	1.08	14.1
19	2	51		1.45×10^8	10.7	1.08	14.1

* Stopped test, specimen did not fail.

TABLE 3c

High Frequency Fatigue Data for Annealed
Titanium 6-2-4-2 at Room Temperature

Specimen Number	Time to Failure			Cycles to Failure N	Stress, ksi	Total Strain Range $\Delta\epsilon$ $\times 10^{-3}$	Freq. KHz
	Hours	Min	Sec				
1			52	6.75×10^5	45.8	5.48	13.0
3			16	2.11×10^5	45.8	5.48	13.0
18			10	1.30×10^5	45.8	5.48	13.0
13		3	58	3.09×10^6	44.3	5.30	13.0
17		24	26	1.03×10^7	44.3	5.30	13.0
20			25	3.25×10^5	44.3	5.30	13.0
9			25	3.25×10^5	42.5	5.09	13.0
10		12	11	9.6×10^6	42.5	5.09	13.0
11			31	4.03×10^5	42.5	5.09	13.0
Chk		11	22	8.82×10^6	40.5	4.85	13.0
4		8	35	6.68×10^6	40.5	4.85	13.0
5		17	25	1.36×10^7	40.5	4.85	13.0
16	4	15		1.98×10^8	39.3	4.71	13.0
19		18	55	1.47×10^7	39.3	4.71	13.0
22	1	21	30	6.32×10^7	39.3	4.71	13.0
7	3	27		1.61×10^8	38.1	4.56	13.0
8	7	6		3.31×10^8	38.1	4.56	13.0
23	5	4		2.36×10^8	38.1	4.56	13.0
15	6	20		2.95×10^8	44.3	5.30	13.0
12	1	37		7.56×10^7	42.5	5.09	13.0
6		1	50	1.43×10^6	38.1	4.56	13.0
21		2	8	1.61×10^5	39.3	4.71	13.0

TABLE 3d
 High Frequency Fatigue Data for Annealed
 Titanium 6-2-4-2 at 900°F

Specimen Number	Time to Failure			Cycles to Failure N	Stress, ksi	Total Strain Range $\Delta\epsilon$ $\times 10^{-3}$	Freq. KHz
	Hours	Min	Sec				
12		1	30	1.21×10^6	31.3	5.21	13.4
13		2	1	1.61×10^6	31.3	5.21	13.4
14		2	15	1.80×10^6	31.3	5.21	13.4
18		3	48	3.06×10^6	30.7	5.12	13.4
19		10	12	8.16×10^6	30.7	5.12	13.4
20		6	53	5.53×10^6	30.7	5.12	13.4
4		33		2.65×10^7	30.1	5.02	13.4
6		23	13	1.81×10^7	30.1	5.02	13.0
7		26	43	2.15×10^7	30.1	5.02	13.4
15	1	55	55	9.25×10^7	29.6	4.93	13.4
16	1	5	45	5.31×10^7	29.6	4.93	13.4
17		59	34	2.87×10^7	29.6	4.93	13.4
9	17	4	45	8.22×10^8	29.0	4.84	13.4
10	3	49		1.84×10^8	29.0	4.84	13.4
11	2	50		1.36×10^8	29.0	4.84	13.4
Chk 2	2	25		1.16×10^8	27.9	4.66	13.4
23	3	13		1.55×10^8	27.9	4.66	13.4
24	7	1		3.38×10^8	27.9	4.66	13.4
21	5	34		2.69×10^8	26.9	4.48	13.4
22	8	15		3.98×10^8	26.9	4.48	13.4
8	20	20		9.80×10^8	26.9	4.48	13.4

HYDRONAUTICS, INCORPORATED

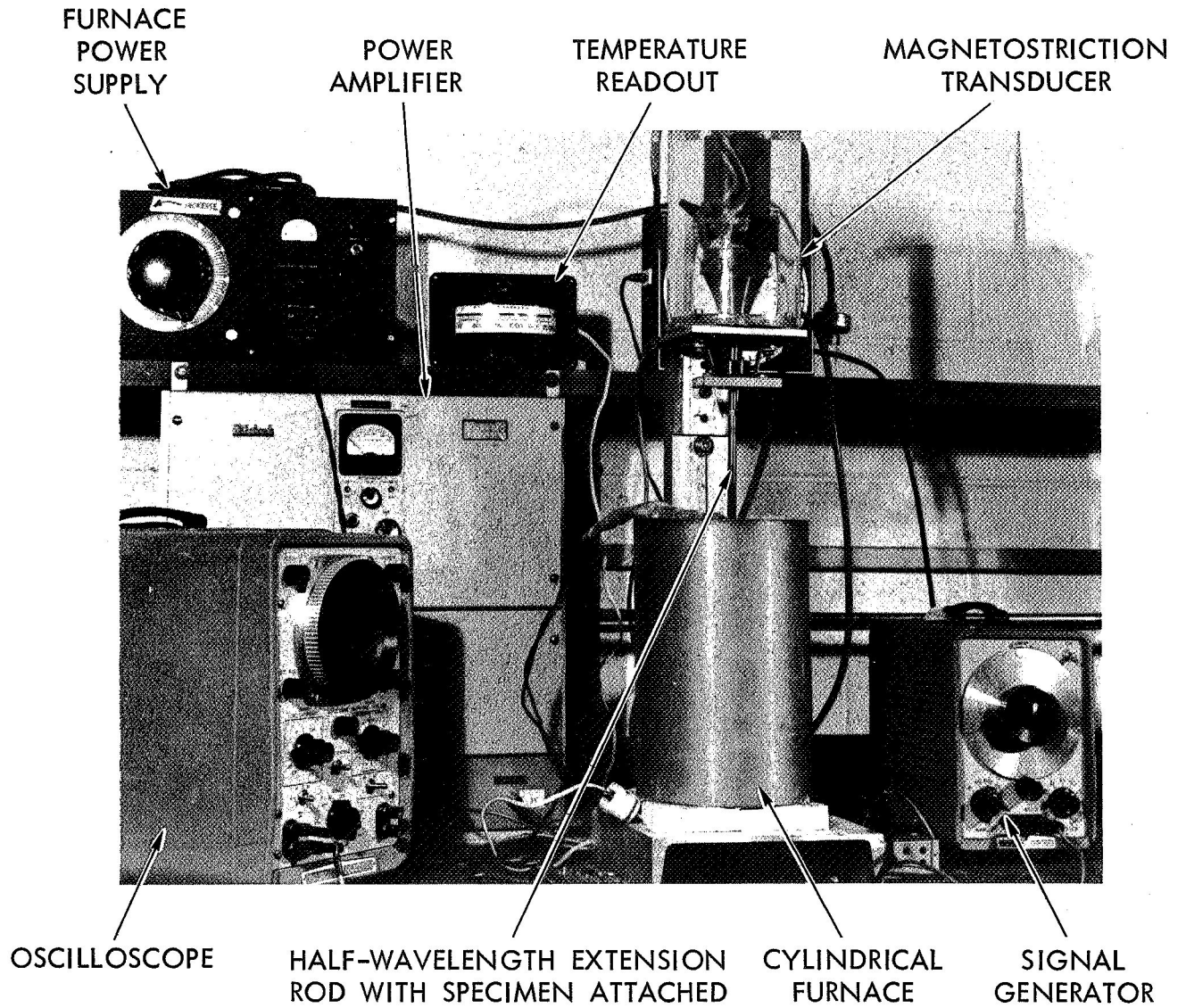


FIGURE 1 - HIGH FREQUENCY FATIGUE APPARATUS WITH
HIGH TEMPERATURE MODIFICATION

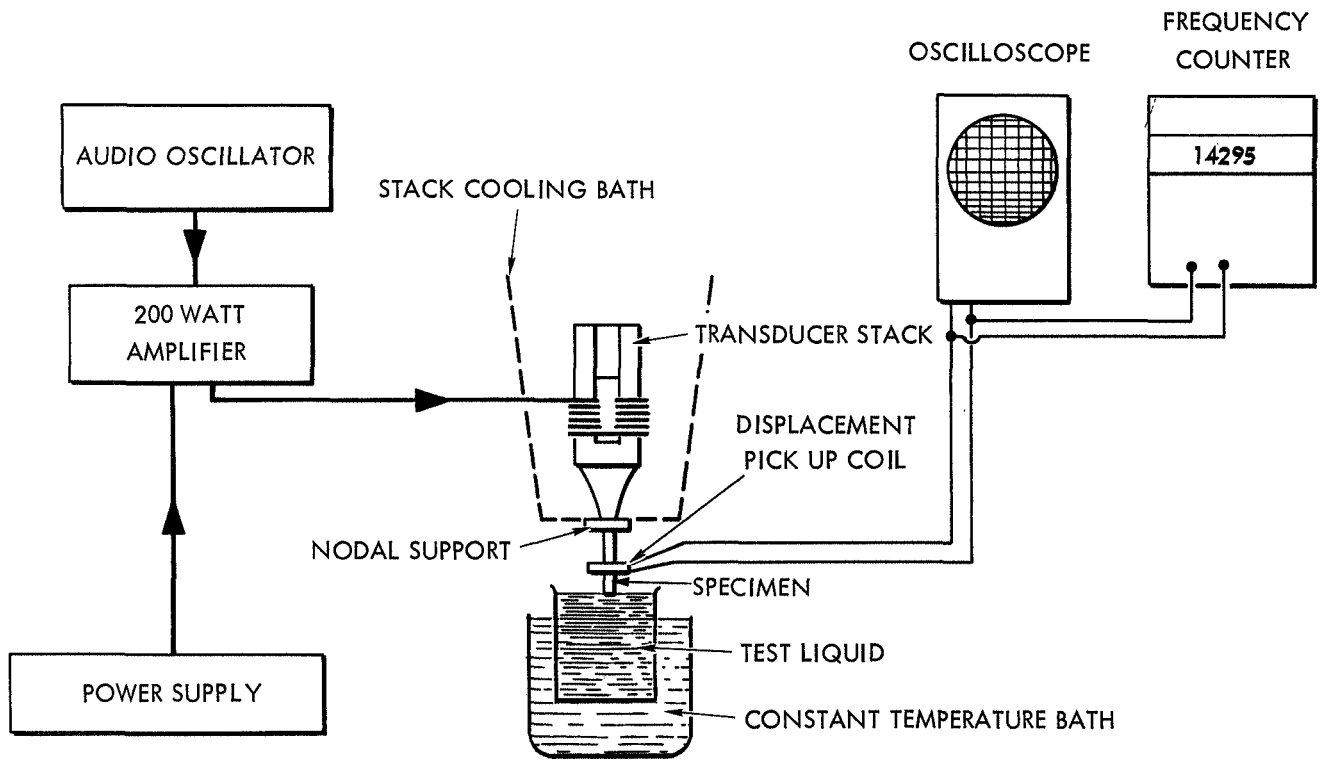
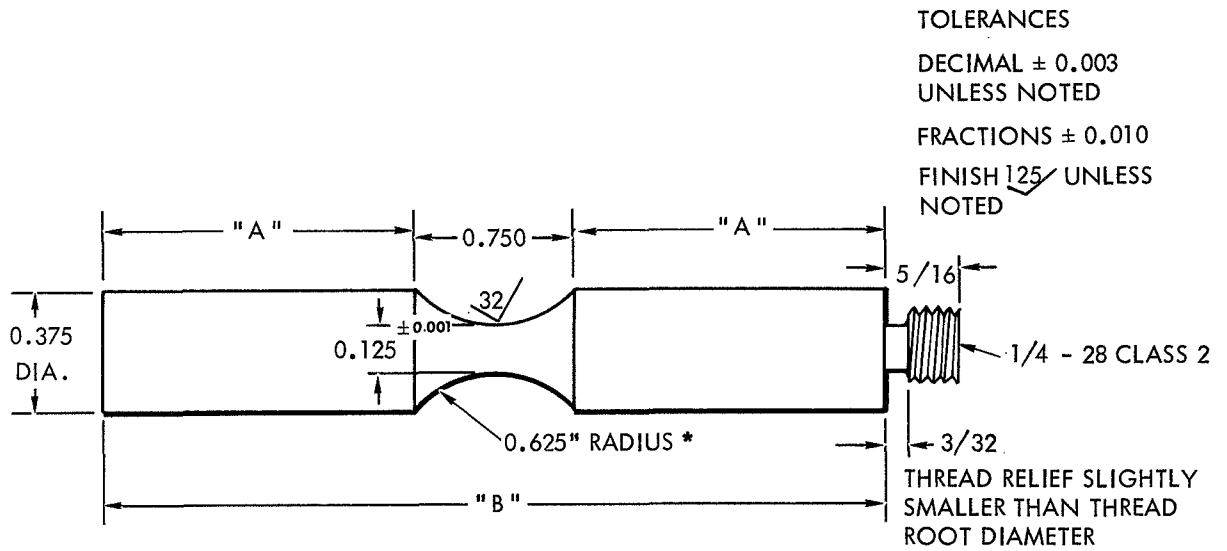


FIGURE 2 - BLOCK DIAGRAM OF THE MAGNETOSTRICTION APPARATUS USED FOR HIGH FREQUENCY FATIGUE TESTS

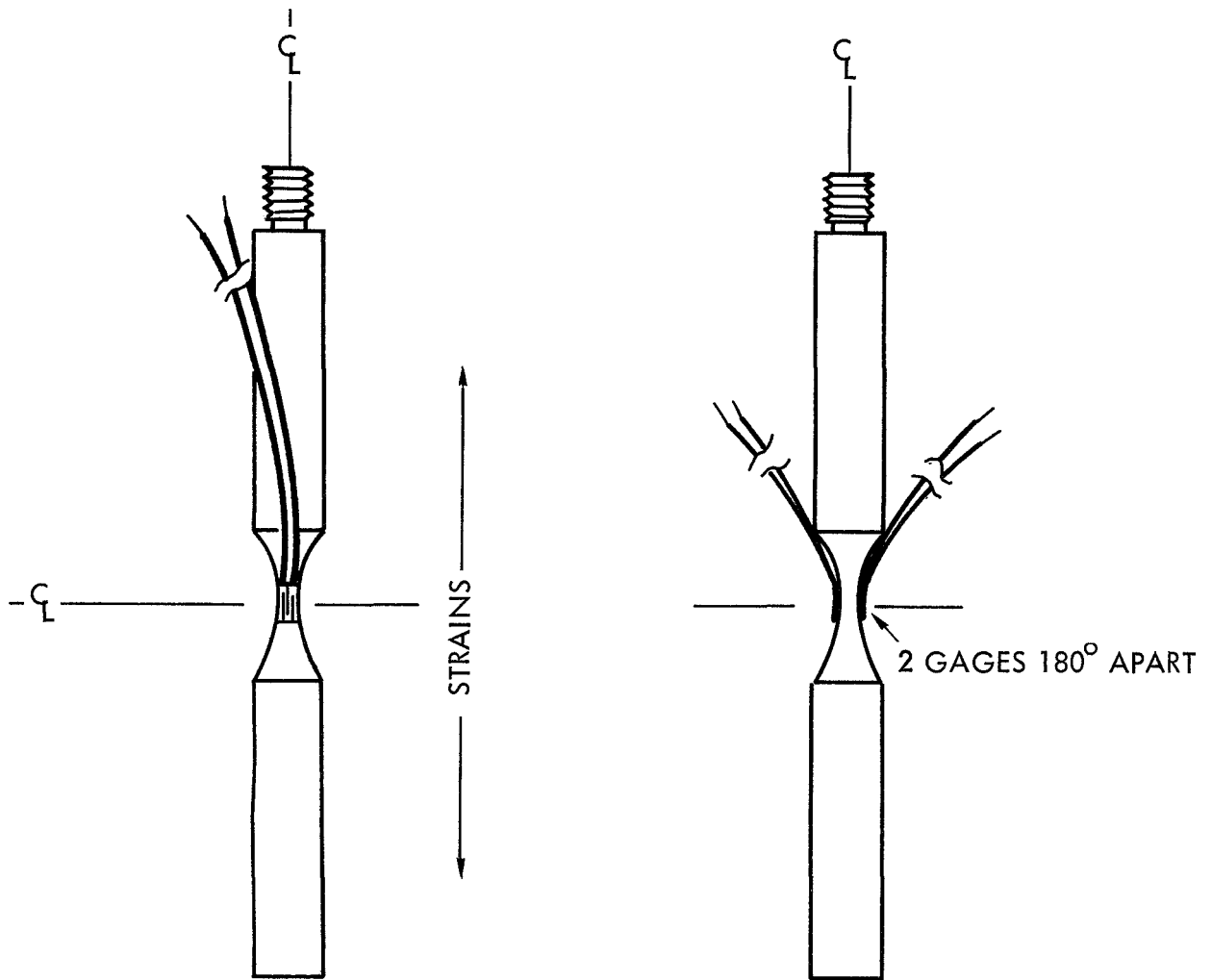
HYDRONAUTICS, INCORPORATED



NOTE * 0.625 RADIUS AREA MUST BE FREE FROM TOOL MARKS AND SCRATCHES TO AT LEAST 32 RMS

MATERIAL	A, in.	B, in.	RESONANT FREQUENCY KHz
316 STAINLESS STEEL RT (ROOM TEMP.)	1.835	4.420	14.2
316 STAINLESS STEEL HT (HIGH TEMP.)	1.492	3.734	14.2
TITANIUM RT 6 Al-2Mo-4Zr-2Sn	2.102	4.954	13.0
TITANIUM HT (SAME)	1.735	4.220	13.0

FIGURE 3 - DUMB-BELL SHAPED HIGH FREQUENCY FATIGUE SPECIMEN



NOTE: REDUCED SECTION HAS 0.625"
RADIUS WITH 0.125" ROOT DIAMETER

FIGURE 4 - STRAIN GAGE ORIENTATION ON FATIGUE
SPECIMEN; BLH TYPE HT-1212-2A

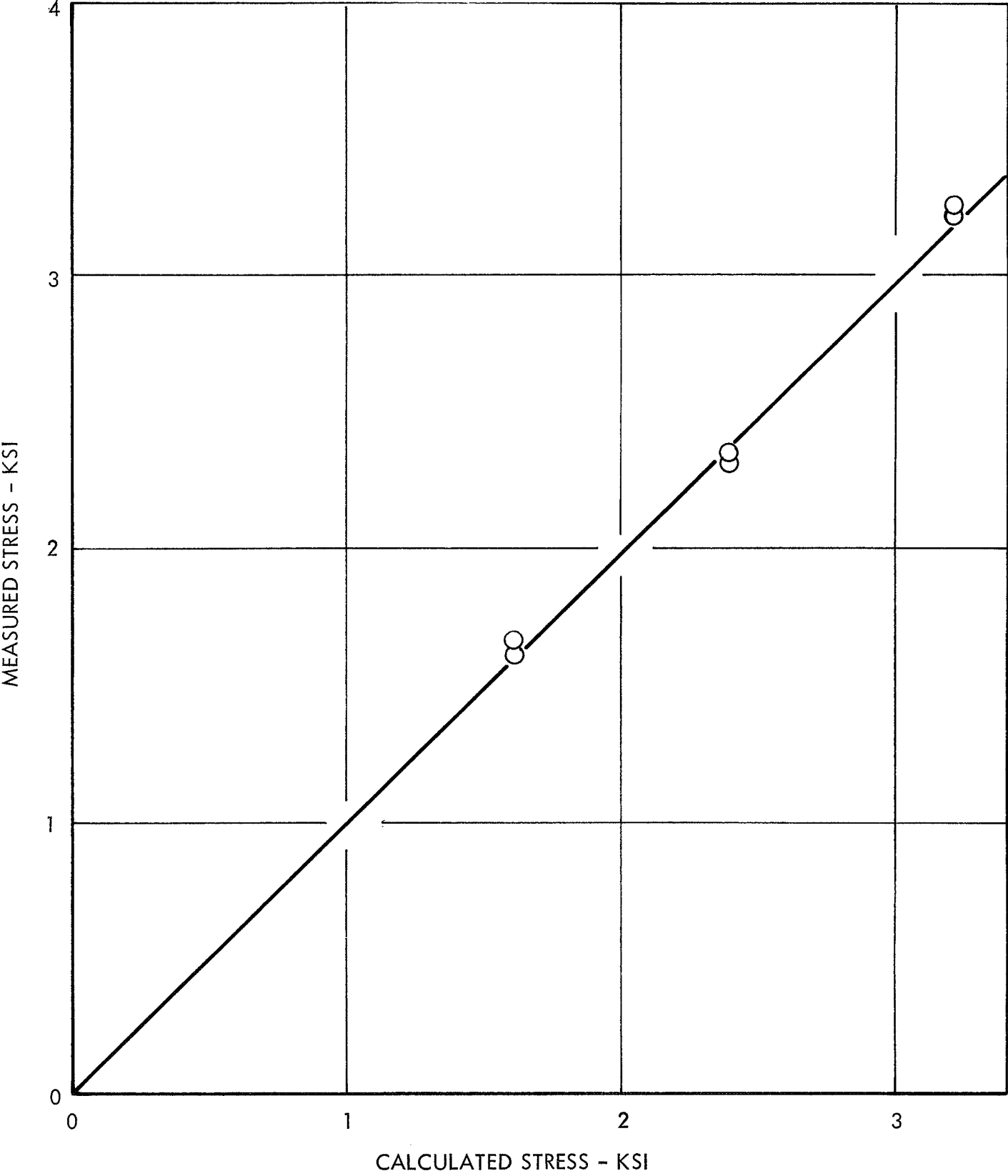


FIGURE 5 - COMPARISON OF DYNAMICALLY MEASURED AND CALCULATED STRESSES IN 316 STAINLESS STEEL FATIGUE SPECIMENS AT 1300° F

HYDRONAUTICS, INCORPORATED

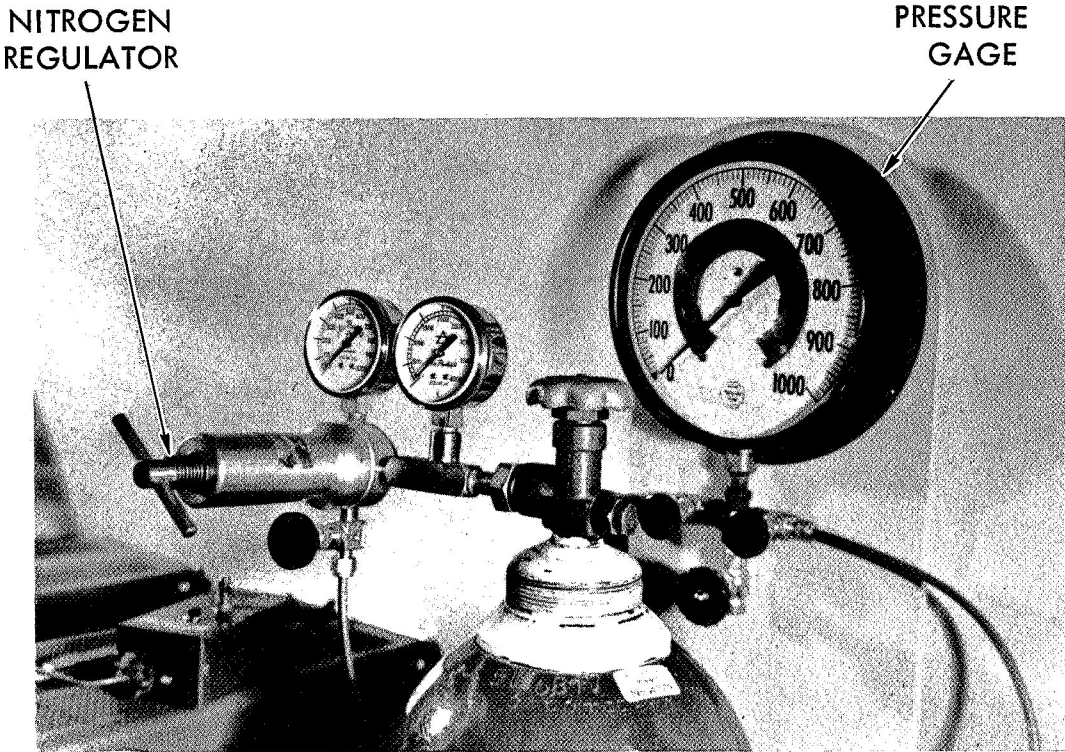
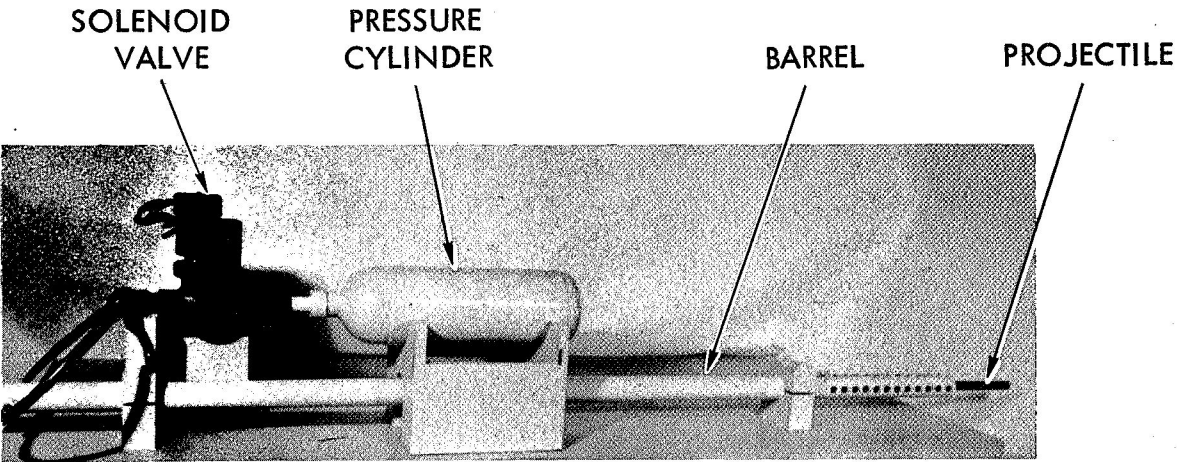


FIGURE 6 - COMPRESSED GAS GUN FOR SPLIT HOPKINSON BAR APPARATUS

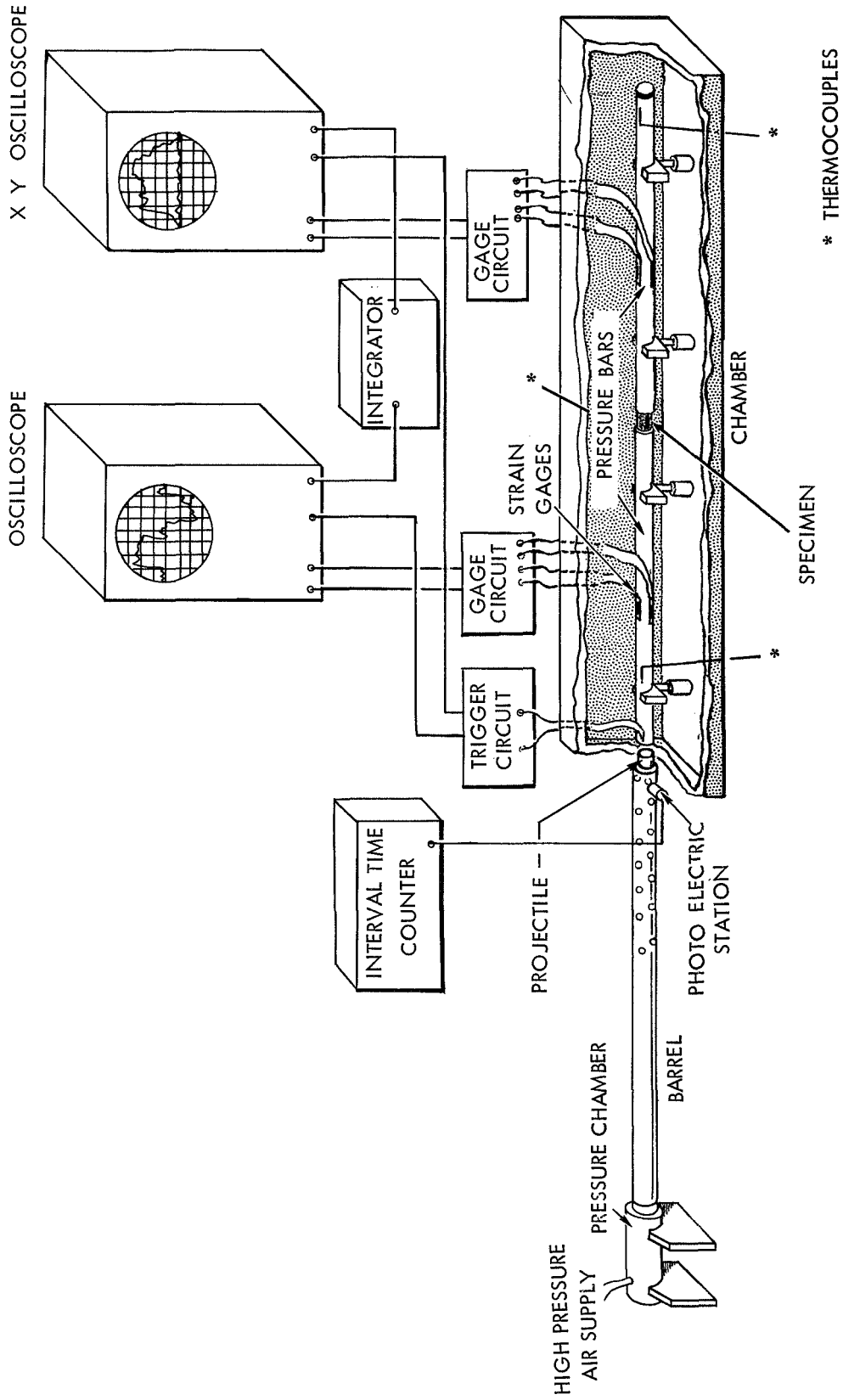


FIGURE 7 - SCHEMATIC OF SPLIT HOPKINSON PRESSURE BAR TEST FACILITY

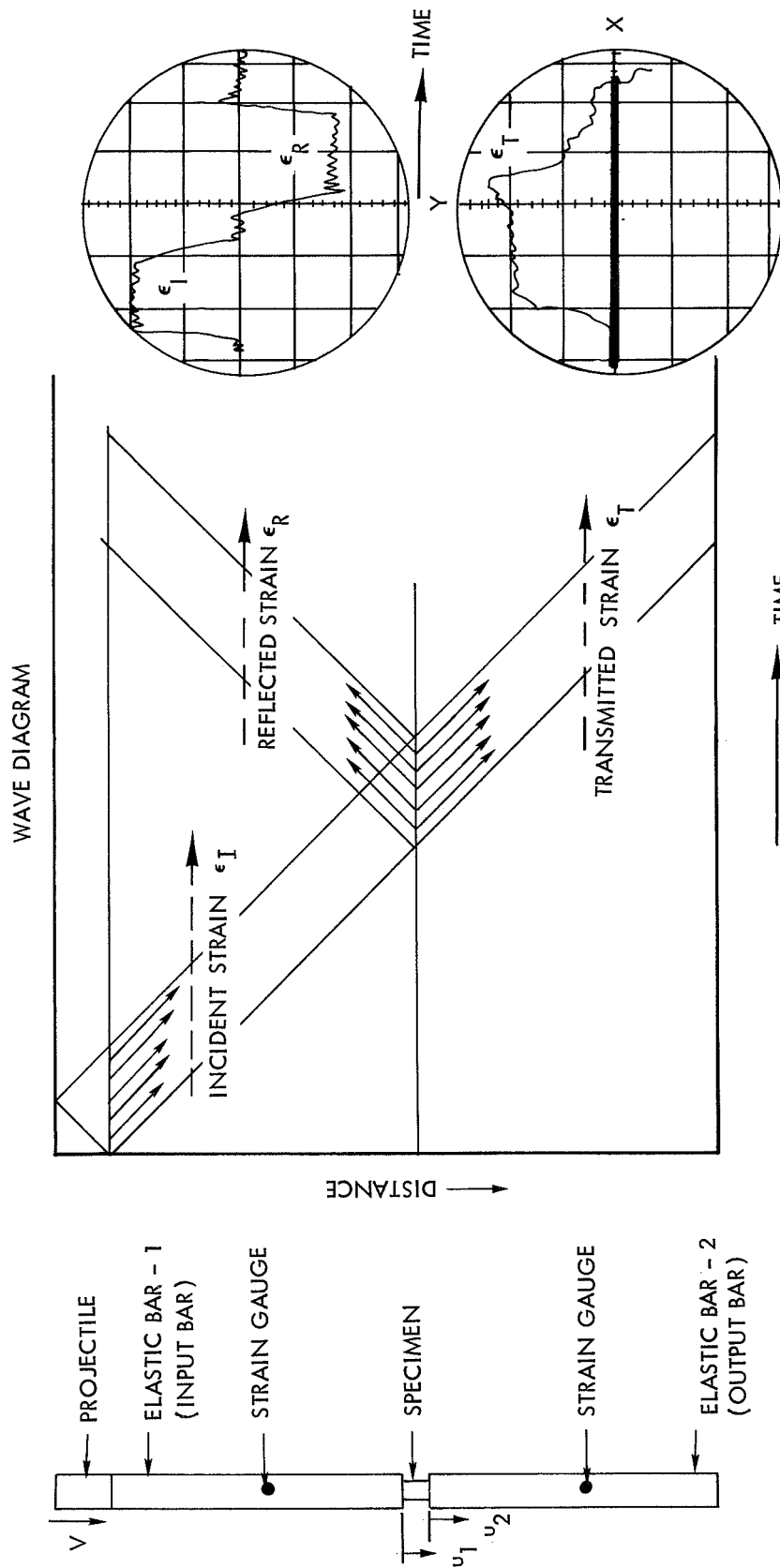
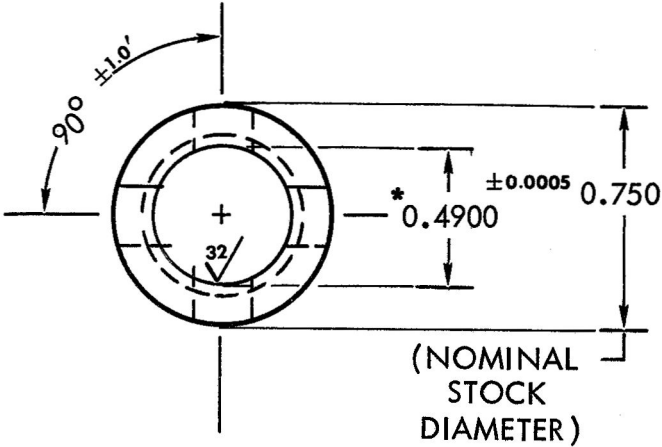
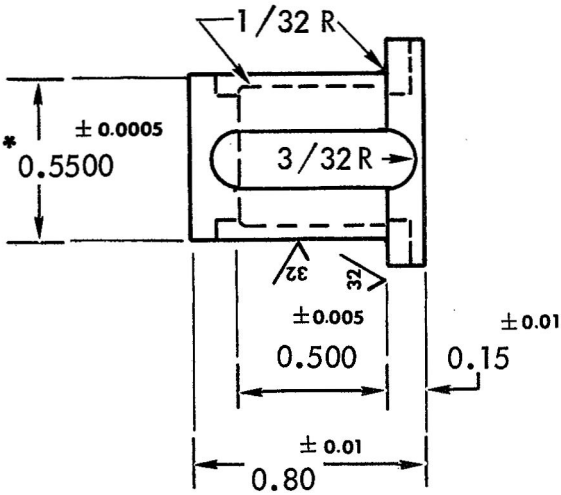
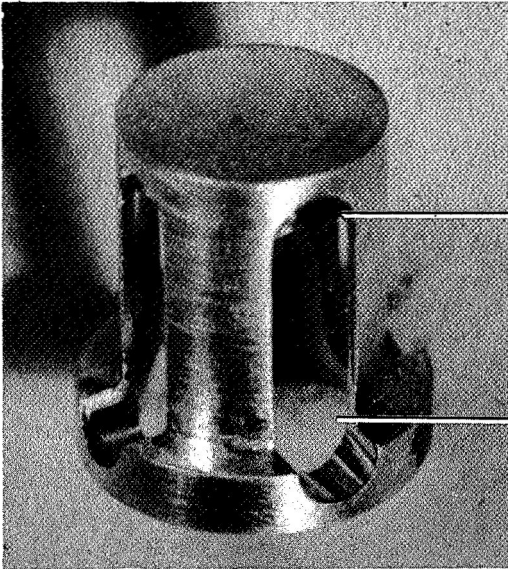


FIGURE 8 - PRINCIPLE OF SPLIT HOPKINSON PRESSURE BAR APPARATUS FOR OBTAINING STRESS-STRAIN DATA AT HIGH STRAIN RATES



NOTE: SURFACE FINISH $\sqrt{32}$
 AS NOTED OTHERS
 125 RPM

* INSIDE AND OUTSIDE DIAMETERS
 TO BE CONCENTRIC TO WITHIN
 ± 0.001 ". AXIAL ALIGNMENT
 (RUNOUT) TO WITHIN 0.001".

FIGURE 9 - HIGH STRAIN RATE TENSILE SPECIMEN

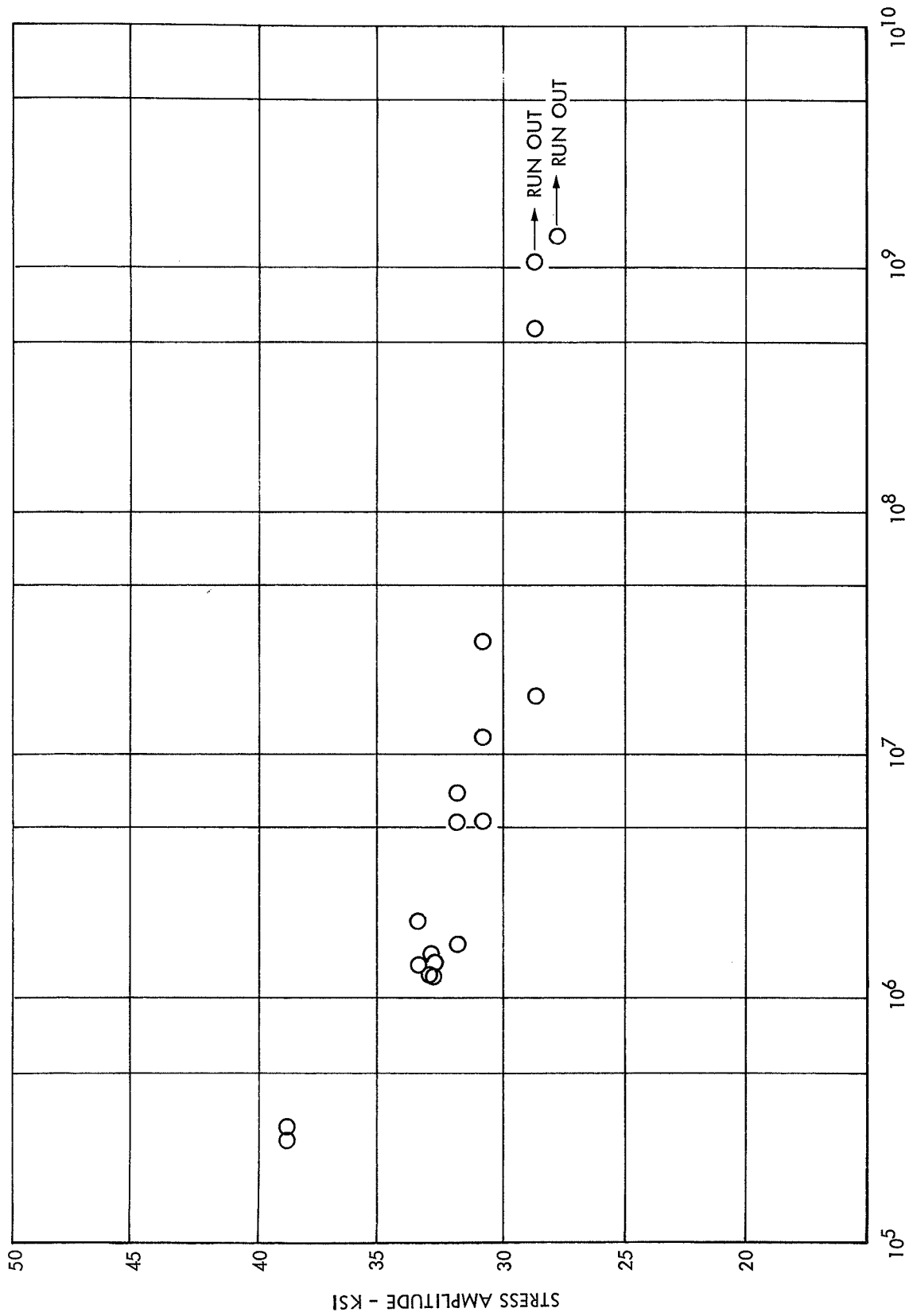


FIGURE 10 - HIGH FREQUENCY FATIGUE DATA FOR ANNEALED 316 STAINLESS STEEL AT ROOM TEMPERATURE

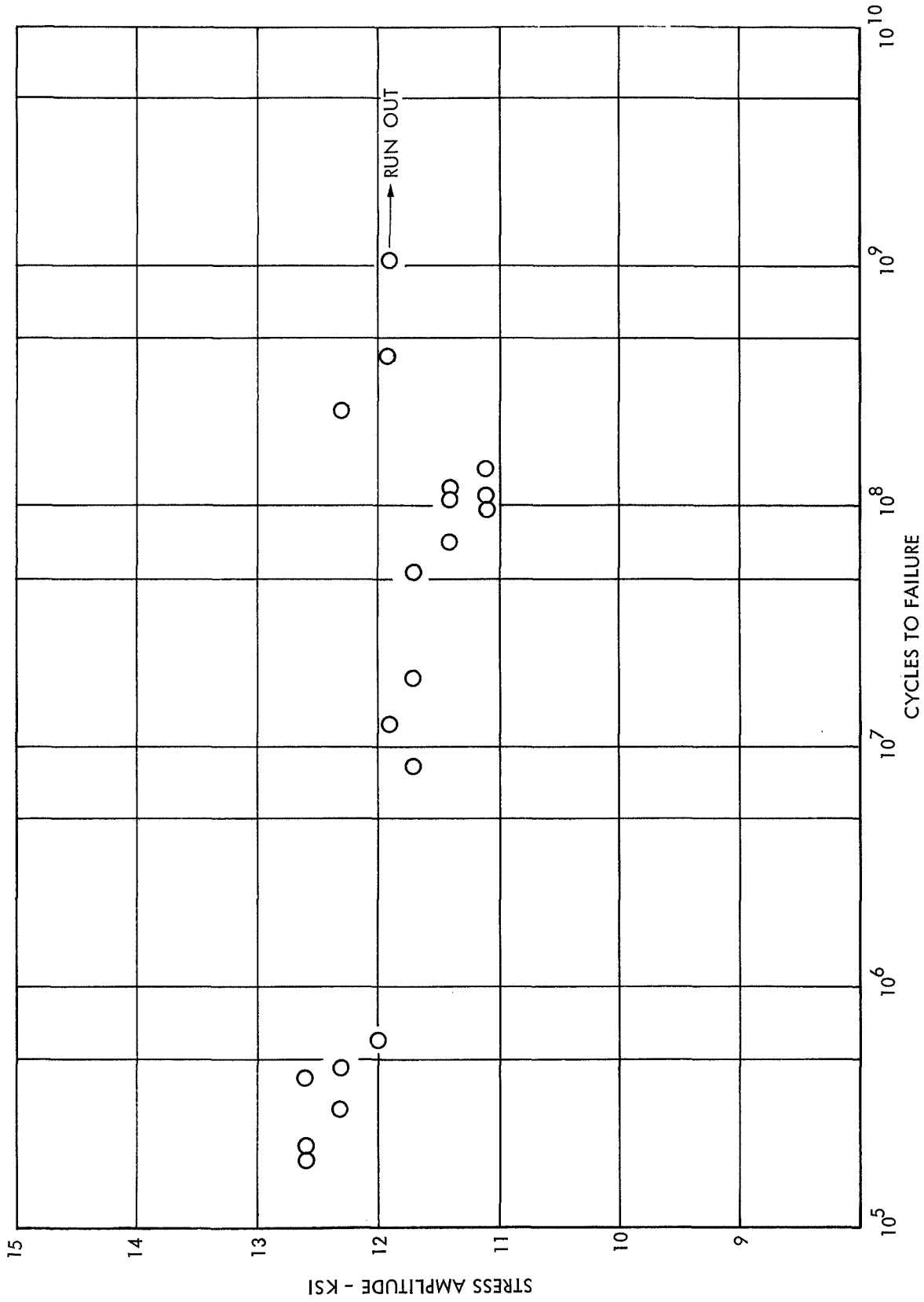


FIGURE 11 - HIGH FREQUENCY FATIGUE DATA FOR ANNEALED 316 STAINLESS STEEL AT 1300° F

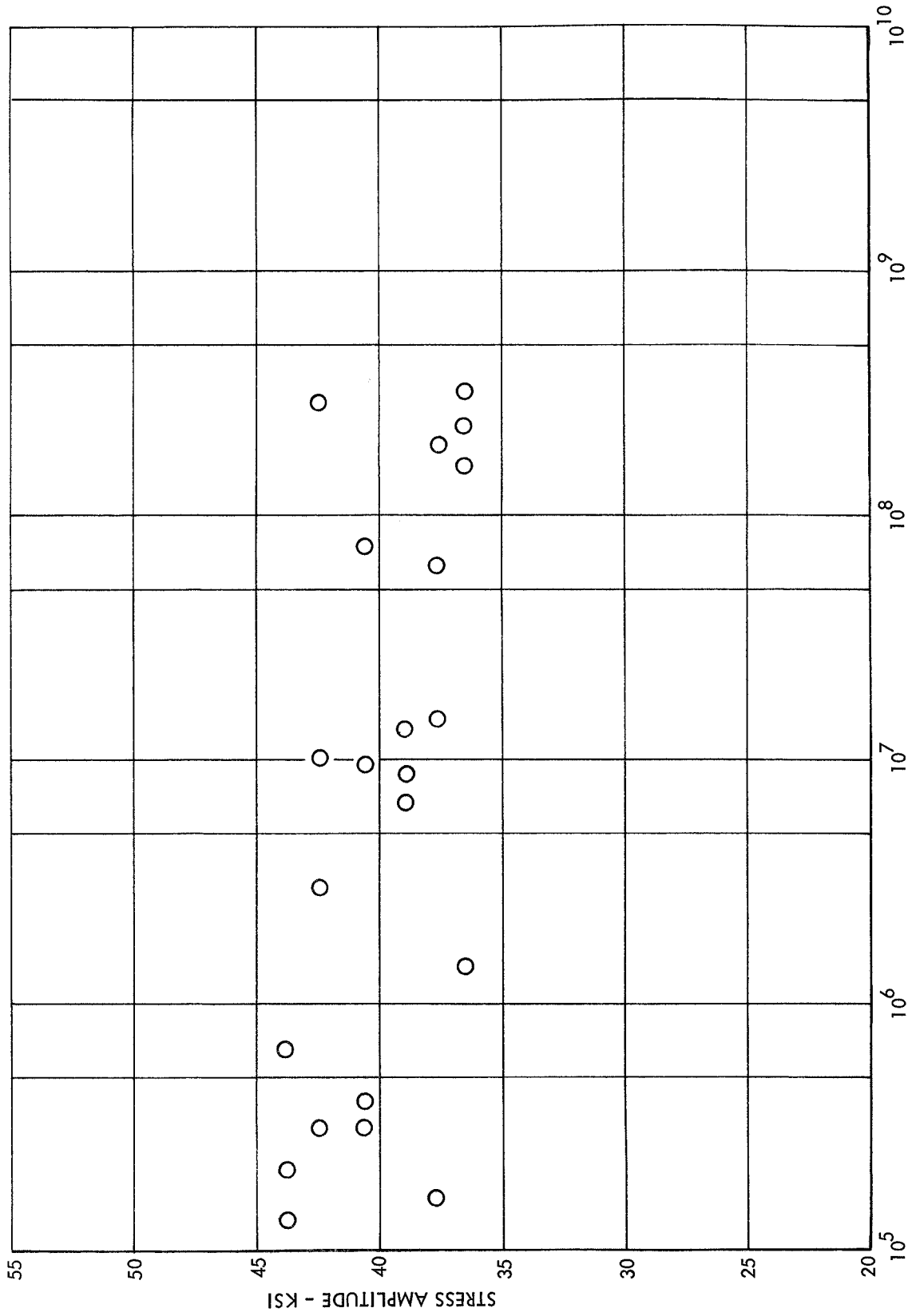


FIGURE 12 - HIGH FREQUENCY FATIGUE DATA FOR TITANIUM - 6 - 2 - 4 - 2 ALLOY AT ROOM TEMPERATURE

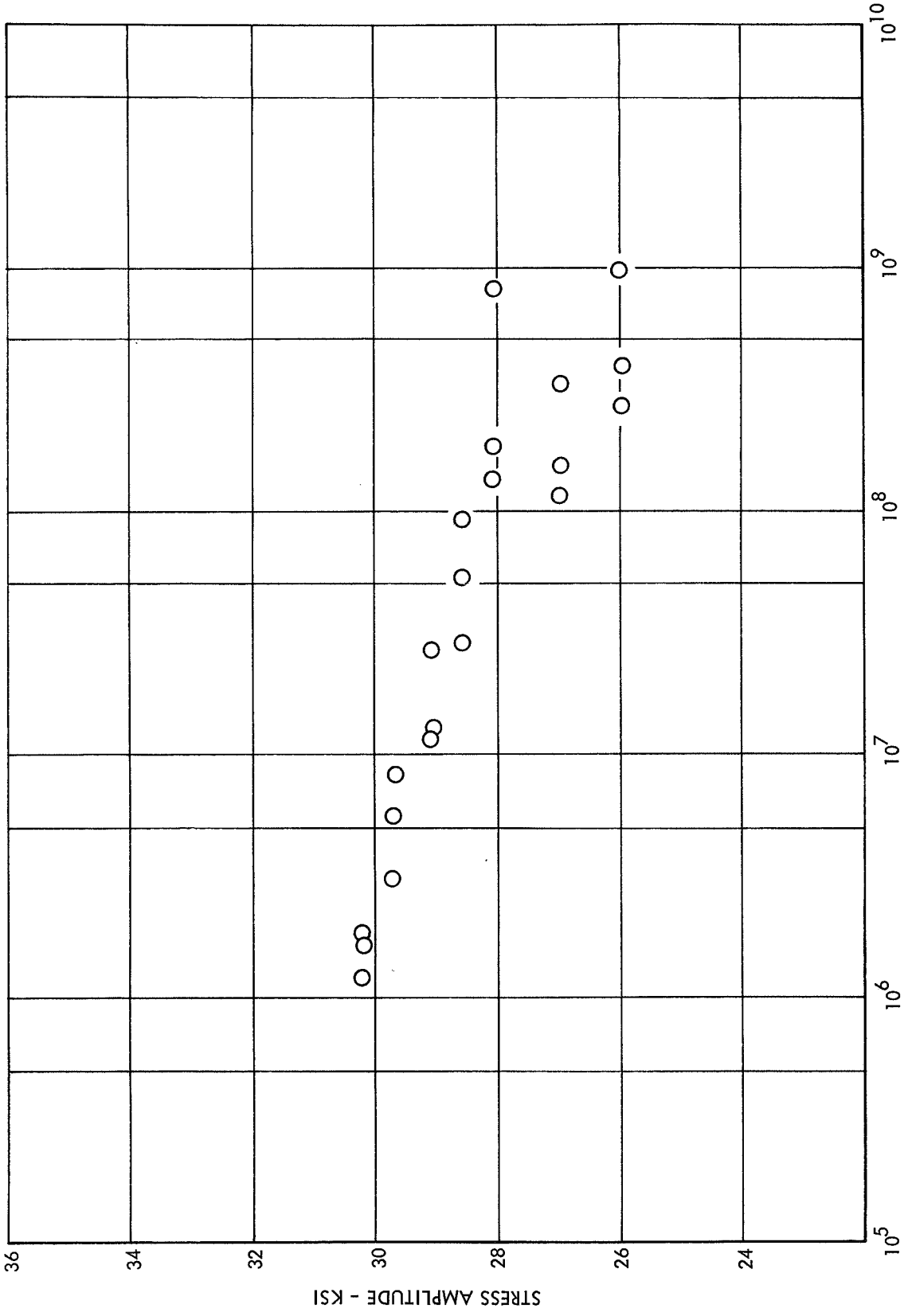


FIGURE 13 - HIGH FREQUENCY FATIGUE DATA FOR TITANIUM - 6 - 2 - 4 - 2 ALLOY AT 900° F

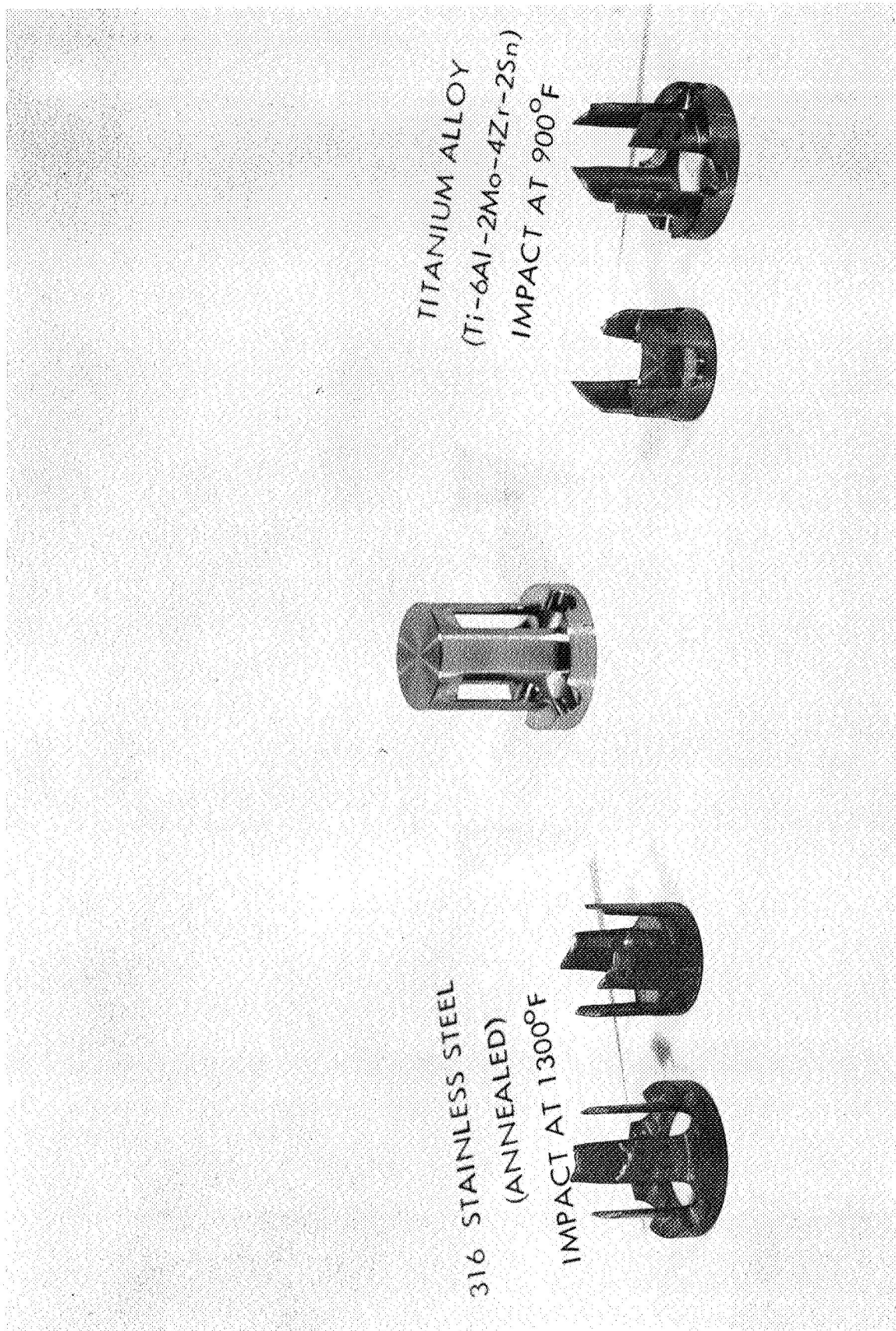


FIGURE 14 - TYPICAL FRACTURED TENSILE SPECIMENS

HYDRONAUTICS, INCORPORATED

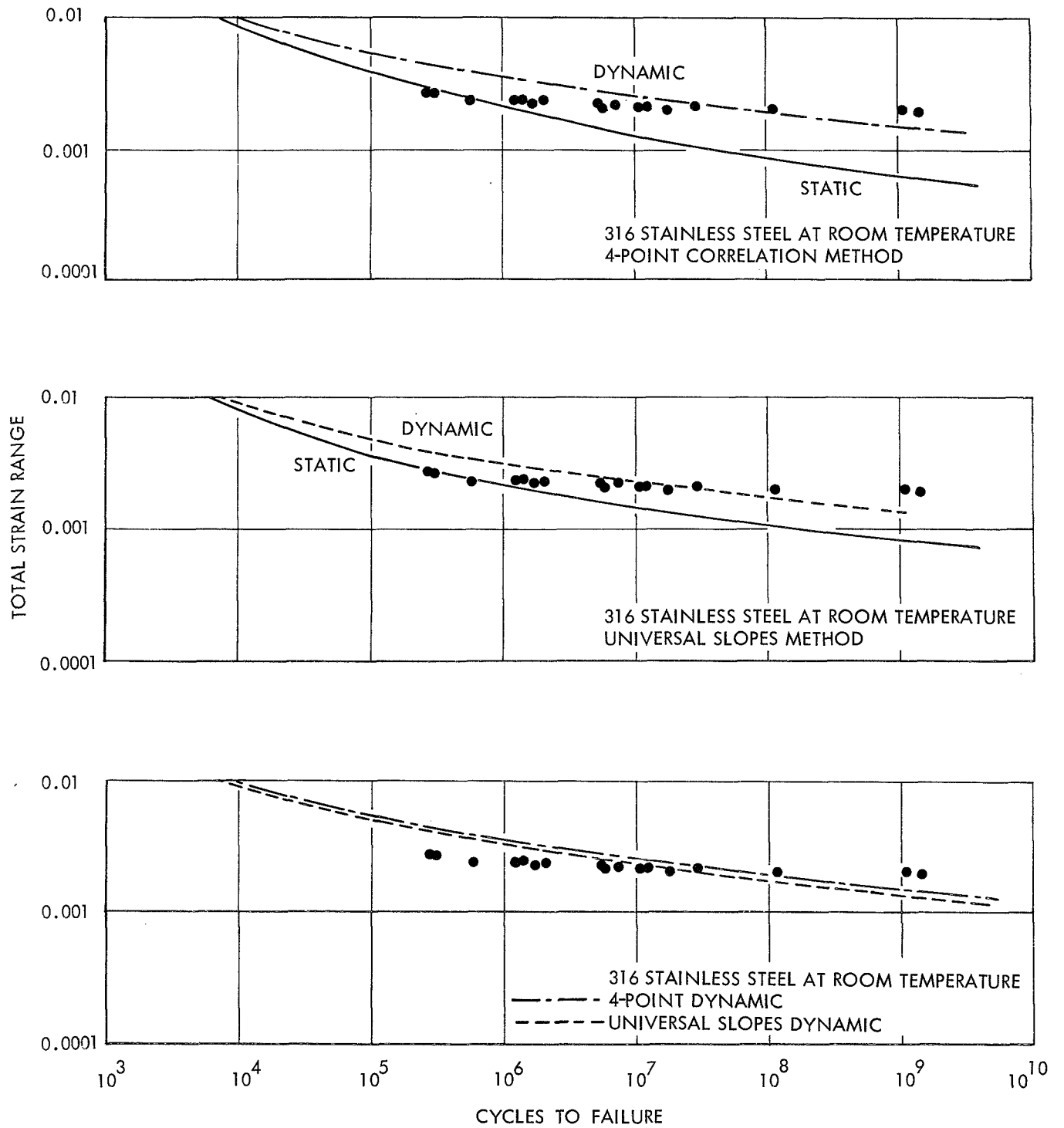


FIGURE 15- COMPARISON OF HIGH FREQUENCY FATIGUE DATA WITH MANSON'S FATIGUE LIFE PREDICTIONS FOR ANNEALED 316 STAINLESS STEEL AT ROOM TEMPERATURE

HYDRONAUTICS, INCORPORATED

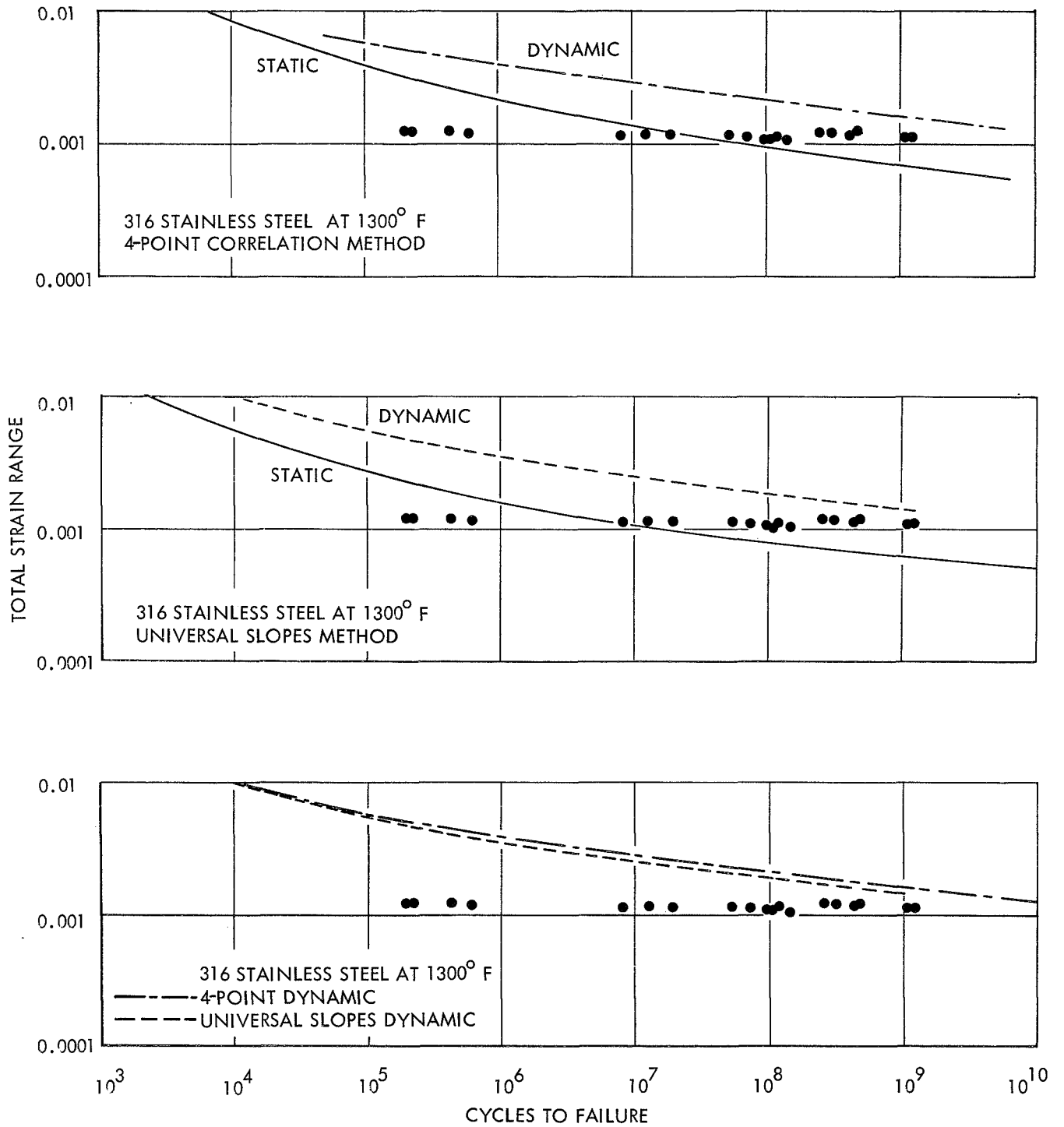


FIGURE 16- COMPARISON OF HIGH FREQUENCY FATIGUE DATA WITH MANSON'S FATIGUE LIFE PREDICTIONS FOR ANNEALED 316 STAINLESS STEEL AT 1300° F

HYDRONAUTICS, INCORPORATED

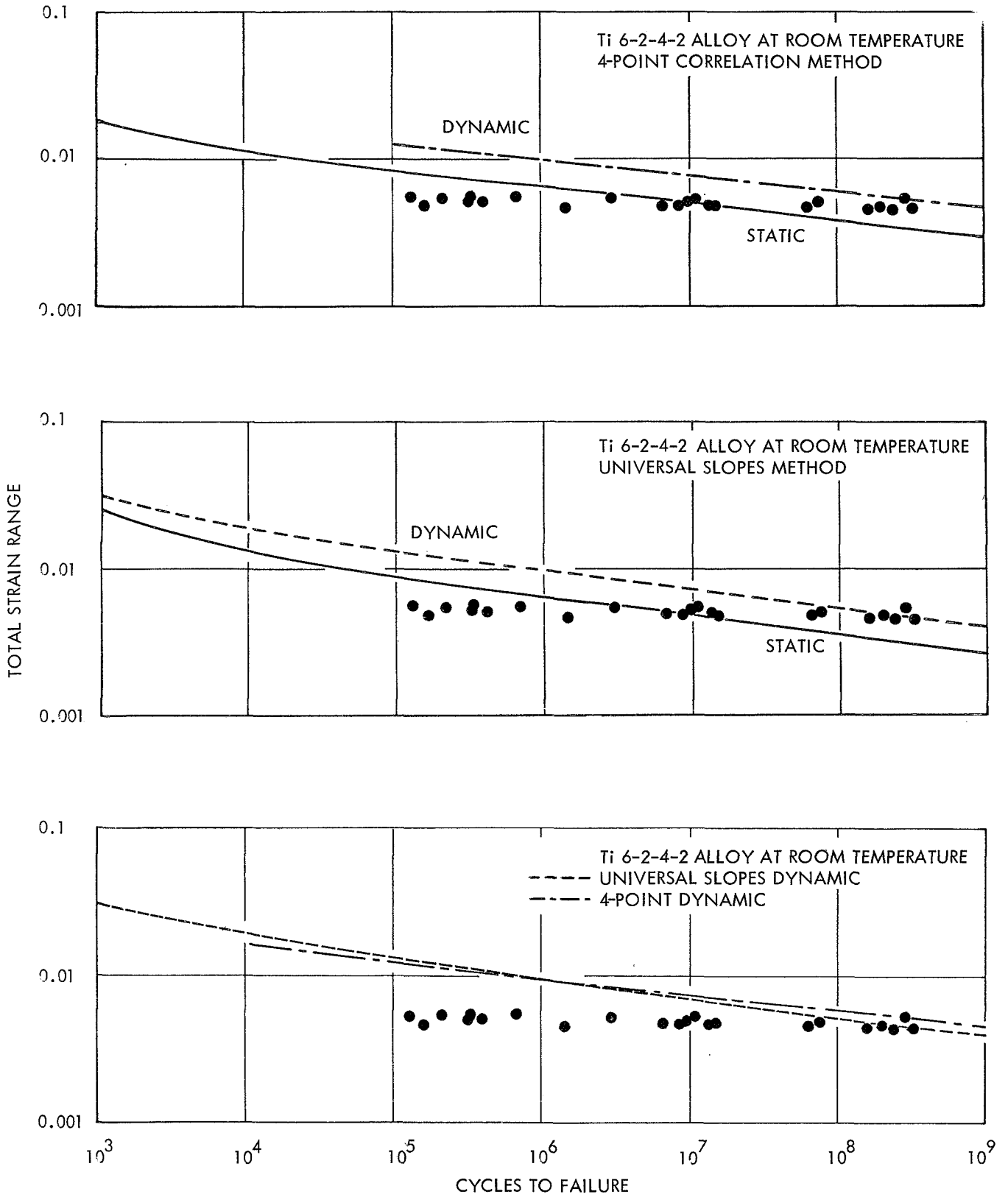


FIGURE 17- COMPARISON OF HIGH FREQUENCY FATIGUE DATA WITH MANSON'S FATIGUE LIFE PREDICTIONS FOR TITANIUM-6-2-4-2 ALLOY AT ROOM TEMPERATURE

HYDRONAUTICS, INCORPORATED

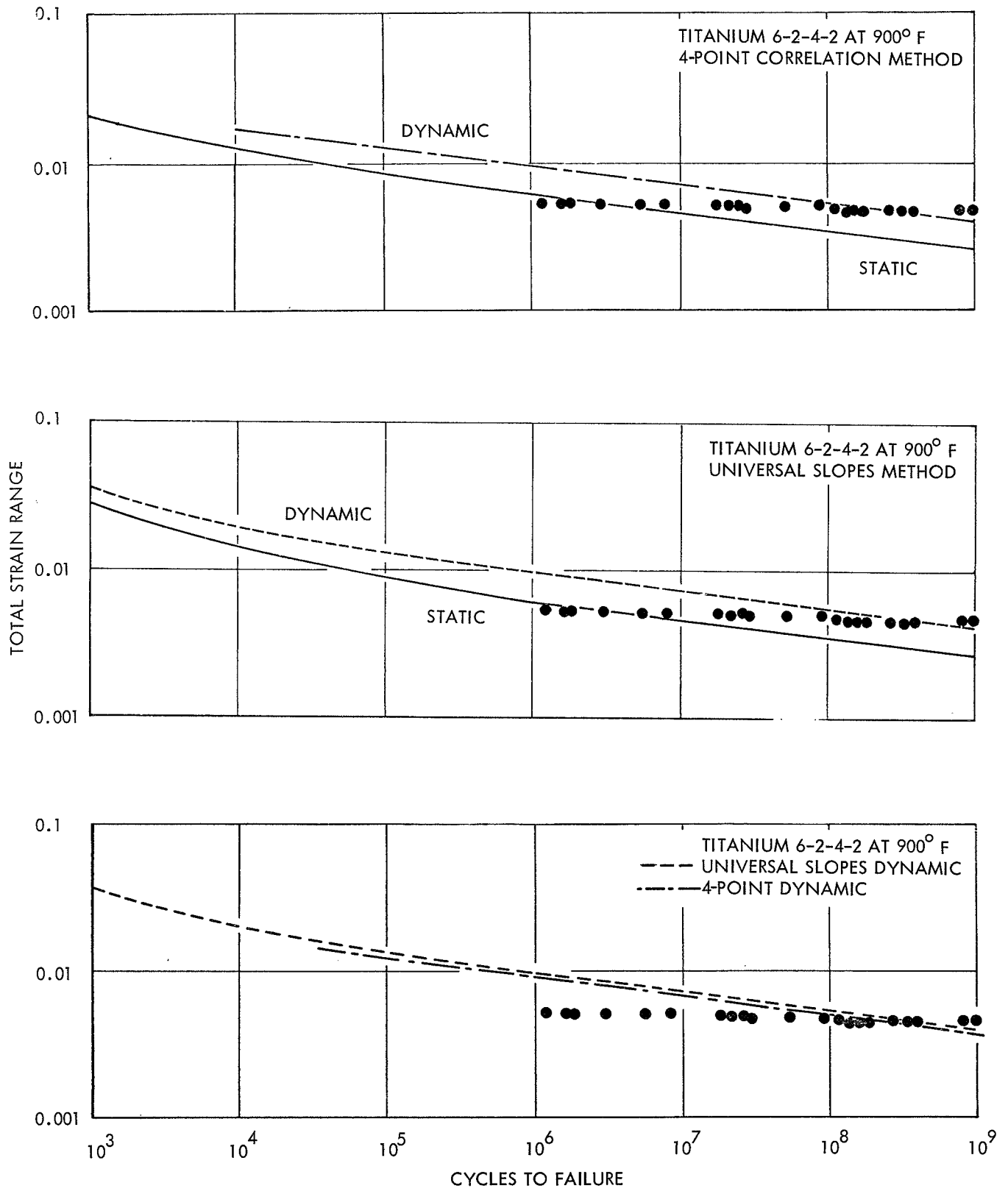
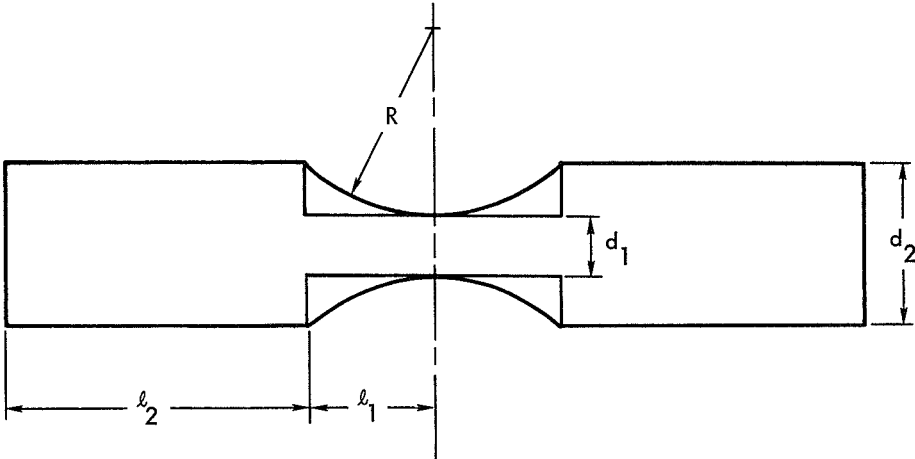


FIGURE 18- COMPARISON OF HIGH FREQUENCY FATIGUE DATA WITH MANSON'S FATIGUE LIFE PREDICTIONS FOR TITANIUM-6-2-4-2 ALLOY AT 900°F



$$\left(\frac{d_2}{d_1}\right)^2 = \text{AREA RATIO}$$

$\frac{l_1}{\lambda}$ AND $\frac{l_2}{\lambda}$ ARE RELATIVE LENGTHS

WHERE λ = WAVE LENGTH OF THE MATERIAL FOR THE TEST FREQUENCY

CURVE OBTAINED FROM NEPPIRAS' THEORY FOR AN AREA RATIO = 9

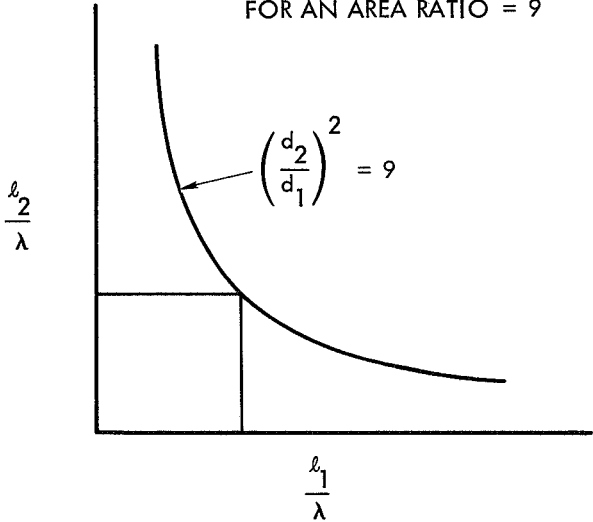


FIGURE 19 - BASIC APPROACH FOR THE DESIGN OF DUMB-BELL SHAPED FATIGUE SPECIMENS

HYDRONAUTICS, INCORPORATED

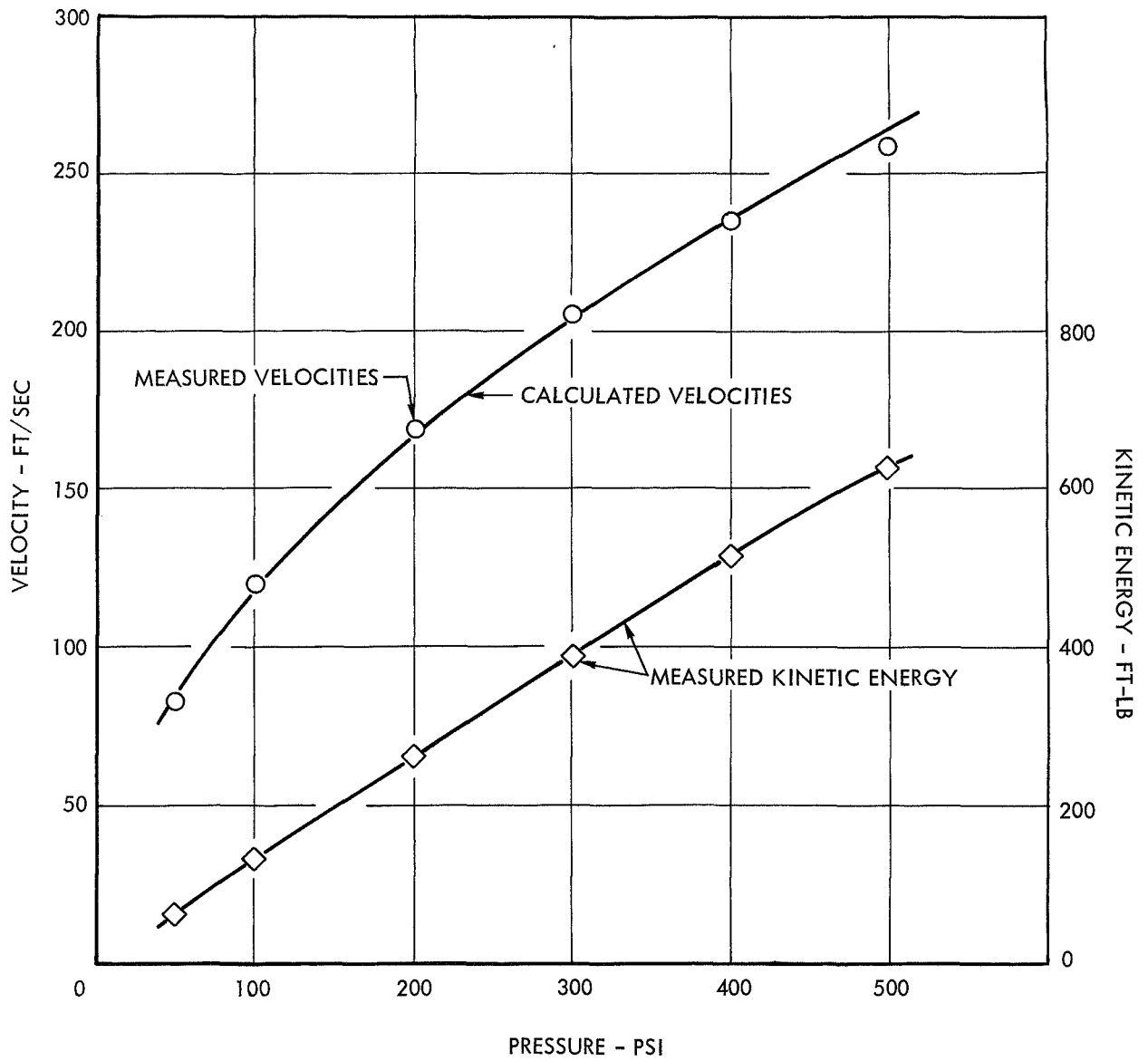


FIGURE 20- COMPRESSED GAS GUN RESPONSE WITH TITANIUM PROJECTILE,
LENGTH: 10.5 IN., DIAMETER: 0.752 IN., WEIGHT: 0.745 LB.

HYDRONAUTICS, Incorporated

-2-

NASA-Langley Research Center Langley Field, Va. 23365 Attn: Richard Pride Library		Department of the Navy ONR, Code 429 1 Washington, D.C. 20525 1 Attn: Dr. R. Roberts 1
NASA Marshall Space Flight Center Huntsville, Alabama 35812 Attn: Library		Chief, Bureau of Naval Weapons Dept. of the Navy 1 Washington, D.C. 20525 Attn: T.F. Kearns RRMA-2 1
NASA Goddard Space Flight Center Greenbelt, Maryland 20771 Attn: D.F. Hasson, Code 714		U. S. Atomic Energy Comm. 1 Washington, D. C. 20545 Attn: Jules Simmons 1 Tech. Rpts. Library 1
NASA Scientific and Technical Information Facility P. O. Box 33 College Park, Md. 20740		Oak Ridge National Lab. 6 Oak Ridge, Tenn. 37830 Attn: Tech. Rpts Library 1
NASA Langley Research Center Langley Field, Va. 23365 Attn: 214/Irvin Miller		Atlantic Research Corp. 1 Shirley Memorial Hwy. Edsel Road Alexandria, Virginia Attn: J.F. Hoeble 1
Headquarters Wright Patterson AFB, Ohio 45433 Attn: AFML/Dr.A.M.Lovelace MAM/Dr.Harris M.Burte		AVCO Lycoming Division 1 505 South Main Street 1 Stratford, Conn. 06497 Attn: W.H. Freeman, Jr. 1
FAA Headquarters 800 Independence Ave.S.W. Washington, D. C. 20553 Attn: Brig.Gen. J.C. Maxwell		American Society for Metals Metala Park 1 Novelty, Ohio 44073 Attn: Dr.Taylor Lyman 1
Department of the Navy NASC Air-5203 Washington, D. C. 20360 Attn: P. Goodwin		Aerospace Corp. Tech. Documents Group 1 P. O. Box 95085 Los Angeles, Calif. 90045 1

HYDRONAUTICS, Incorporated

-3-

Defense Metals Inf. Center (DMIC) Battelle Memorial Institute 505 King Avenue Columbus, Ohio 43201	1	Ford Motor Company Materials Development Dept. 20000 Rotunda Drive P. O. Box 2053 Dearborn, Mich. 48123 Attn: Mr. Y.P. Telang	1
The Bendix Corporation Research Laboratories Div. Southfield, Michigan 48075 Attn: Library	1	General Electric Co. Materials Dev. Lab. Opera. Advance Engine and Tech. Dept. Cincinnati, Ohio 45215 Attn: L.P. Jahnke	1
Boeing Company P.O. Box 733 Renton, Washington 98055 Attn: W.E. Binz, SST Unit Chief	1	General Electric Co. Advanced Technology Lab. Schnectady, N.Y. 12305 Attn: Library	1
Battelle Memorial Institute 505 King Avenue Columbus, Ohio 43201 Attn: Dr.R.I. Jaffee	1	General Electric Co. Re-entry and Environmental Systems Div. Valley Forge Space Tech. Center P. O. Box 8555 Philadelphia, Penn. 19101	1
Douglas Aircraft Co. MFSD 3000 Ocean Park Bld. Santa Monica, Calif. 90406 Attn: Library	1	General Motors Corp. Allison Division Indianapolis, Ind. 46206 Attn: D.K. Hanink Materials Lab.	1
Denver Research Institute University Park Denver, Colorado 80210 Attn: Library	1	General Technologies Corp. 1821 Michael Faraday Drive Reston, Virginia 22070 Attn: Dr. R.G. Shaver Vice President, Engr.	1
General Technologies Corp. 708 North West Street Alexandria, Va. 22314 Attn: Library	1	IIT Research Institute Technology Center Chicago, Ill. 60616 Attn: S.L. Blum	1

HYDRONAUTICS, Incorporated

-4-

IIT Research Institute Technology Center Chicago, Illinois 60616 Attn: Mr.V. Hill Library	1 1	Stanford University Palo Alto, Calif. 94305 Attn: Library	1
University of Illinois Department of Ceramic Engr. Urbana, Illinois 61801 Attn: Mr. J. Wurst	1	United Aircraft Corporation 400 Main Street East Hartford, Conn. 06108 Attn: Research Library E. F. Bradley, Chief Materials Engr.	1 1
Lockheed Palo Alto Res. Labs. Materials and Science Lab.52-30 3251 Hanover Street Palo Alto, Calif. 94304 Attn: Tech. Inf. Center	1	United Aircraft Corporation Pratt and Whitney Division West Palm Beach, Fla. 33402 Attn: Library	1
Ohio State University Columbus, Ohio 43210 Attn: Prof. R.A. Rapp Dept. of Metall. Engr.	1	University of Dayton Research Institute 300 College Park Avenue Dayton, Ohio 45409 Attn: Library	1
Michigan Technical University Houghton, Michigan 49931 Attn: Prof. R. W. Guard, Head Dept. of Metallurgical Engineering	1	Westinghouse Electric Corp. MacArthur Avenue. Bloomfield, N.J. 07003 Attn: Library	1
University of Pittsburgh Center for Study of Thermo- dynamic Properties of Materials 409 Engineering Hall Pittsburgh, Penn. 15213 Attn: Dr.G.R. Fitterer	1	Wah Chang Corporation Albany, Oregon 97321 Attn: Library	1
TRW Electromechanical Div. TRW Inc. 23555 Euclid Avenue Cleveland, Ohio 44117 Attn: Library	1	Westinghouse Electric Corp. Research Laboratories Beulah Road, Churchill Buro. Pittsburgh, Penn. 15235 Attn: Mr.R. Grekila	1
		Universal-Cyclops Steel Corp. Bridgeville, Penn. 15017 Attn: Library	1